In Situ Observations of Ions and Magnetic Field Around Phobos: The Mass Spectrum Analyzer (MSA) for the Martian Moons eXploration (MMX) Mission

Shoichiro Yokota (yokota@ess.sci.osaka-u.ac.jp)
Osaka Univ. https://orcid.org/0000-0001-8851-9146

Naoki Terada
Tohoku University

Ayako Matsuoka
Kyoto University: Kyoto Daigaku

Naofumi Murata
JAXA

Yoshifumi Saito
ISAS/JAXA

Dominique Delcourt
LPP-CNRS-Sorbonne

Yoshifumi Futaana
Swedish Institute of Space Physics

Kanako Seki
The University of Tokyo: Tokyo Daigaku

Micah J Schaible
Georgia Institute of Technology

Kazushi Asamura
ISAS/JAXA

Satoshi Kasahara
The University of Tokyo: Tokyo Daigaku

Hiromu Nakagawa
Tohoku University: Tohoku Daigaku

Masaki N Nishino
ISAS/JAXA

Reiko Nomura
ISAS/JAXA

Kunihiro Keika
The University of Tokyo: Tokyo Daigaku

Yuki Harada
Kyoto University: Kyoto Daigaku
Shun Imajo
Nagoya University: Nagoya Daigaku

Full paper

Keywords: Martian Moons eXploration (MMX), Phobos, Mars, mass spectrum analyzer, magnetometer

Posted Date: December 21st, 2020

DOI: https://doi.org/10.21203/rs.3.rs-130696/v1

Version of Record: A version of this preprint was published at Earth, Planets and Space on December 1st, 2021. See the published version at https://doi.org/10.1186/s40623-021-01452-x.

In situ observations of ions and magnetic field around Phobos: The Mass Spectrum Analyzer (MSA) for the Martian Moons eXploration (MMX) mission

Shoichiro Yokota[1], Naoki Terada[2], Ayako Matsuoka[3], Naofumi Murata[4], Yoshifumi Saito[5], Dominique Delcourt[6], Yoshifumi Futaana[7], Kanako Seki[8], Micah J. Schaible[9], Kazushi Asamura[5], Satoshi Kasahara[8], Hiromu Nakagawa[2], Masaki N. Nishino[5], Reiko Nomura[5], Kunihiro Keika[8], Yuki Harada[3], Shun Imajo[10]

1) Osaka University, Machikaneyama-cho, Toyonaka, Japan, 560-0043
2) Tohoku University, Aoba-ku, Sendai, Japan, 980-8578
3) Kyoto University, Kitashirakawaoiwake-cho, Sakyo-ku, Kyoto, Japan, 606-8502
4) Japan Aerospace Exploration Agency, Tsukuba, Ibaraki, Japan, 305-8505
5) Institute of Space and Astronautical Science, Japan Aerospace Exploration Agency, Yoshinodai, Chuo-ku, Sagamihara, Japan, 252-5210
6) LPP-CNRS-Sorbonne Universite-Ecole Polytechnique, 4 place Jussieu, 75252 Paris, France
7) Swedish Institute of Space Physics, Box 812, SE-98128 Kiruna, Sweden.
8) The University of Tokyo, Hongo, Bunkyo-ku, Japan, 113-0033
9) Georgia Institute of Technology, 901 Atlantic Drive, Atlanta, GA 30332
10) Nagoya University, Furo-cho, Chikusa-ku, Nagoya, Japan, 464-8601

Indicate the corresponding author Shoichiro Yokota (yokota@ess.sci.osaka-u.ac.jp)

Abstract

The Mass Spectrum Analyzer (MSA) will perform in-situ observations of ions and magnetic fields around Phobos as part of the Martian Moons eXploration (MMX) mission to investigate the origin of the Martian moons and physical processes in the Martian environment. MSA consists of an ion energy mass spectrometer and two magnetometers which will measure velocity distribution functions and mass/charge distributions of low-energy ions and magnetic field vectors, respectively. For the MMX scientific objectives, MSA will observe solar wind ions, those scattered at the Phobos surface, water-related ions generated in the predicted Martian gas torus, secondary ions sputtered from Phobos, and escaping ions from the Martian atmosphere, while monitoring the surrounding magnetic field. MSA will be developed from previous instruments for space plasma missions such as Kaguya, Arase, and BepiColombo/Mio to contribute to the MMX scientific objectives.

Keywords

Martian Moons eXploration (MMX), Phobos, Mars, mass spectrum analyzer, magnetometer

Main Text

1. Introduction

Mars and Earth are terrestrial planets with moons in the inner solar system. When studying the origin and evolution of the Earth and the Moon, it is essential to treat the two bodies together as the Earth-Moon system, because lunar explorations and analyses of the returned Apollo and Luna samples and meteorites have revealed a history of Earth-Moon co-evolution (e.g., Taylor et al. 2006). The results of these studies have led to the theory of a giant impact on the birth of the Moon (Canup & Asphang, 2001) and the transport of the early Earth's atmosphere to the Moon (Ozima et al., 2005; 2008). The Earth's atmosphere currently leaks into space (Seki et al., 2001) and some of them have been implanted inside the lunar surface materials since billions of years ago (Terada et al., 2017).

The formation and evolution of Mars have also been studied from observations by both orbiters (e.g., Albee et al., 2001; Wilson, 2004; Jakosky et al., 2015) and landers/rovers (e.g., Grotzinger et al. 2012), and analyses of Martian meteorites (e.g., Agee et al., 2013,

Borg et al., 2005). Although our understanding of Mars is improving, that of the Martian moons is greatly limited due to the lack of information obtained from spacecraft observations and analyses of meteorites from the moons. Similar to previous controversies about the origin of Earth's Moon, several theories have been proposed for the birth of the Martian moons that involve either the collision of large objects with Mars (e.g., Rosenblatt et al., 2016) or the capture of asteroids (e.g., Higuchi & Ida, 2017). Moreover, Martian orbiter observations suggested that the large amount of Martian atmosphere has escaped over Mars' history (e.g., Barabash et al., 2007; Jakosky et al., 2017) and can influence the Phobos' surface, predominantly through oxygen ion irradiation (Nenon et al., 2019).

Because the Martian moons are still a missing piece to our understanding of the evolution of the solar system, a Martian Moons eXploration (MMX) mission is scheduled, which will conduct remote-sensing, in-situ measurements and sample return similarly to Hayabusa 1 and 2 (Fujiwara et al. 2006; Watanabe et al. 2019). The science objectives are not only to reveal the origin of the Martian moons but also to understand physical processes in the Martian environment for investigating co-evolution of the Martian-moons system (Kuramoto et al., this issue).

In the MMX mission, it is planned to perform in-situ observations of ions as a key objective. Ions in the Martian environment can come from Mars' atmosphere, sputtering and stimulated desorption from the moons, photoionization of the predicted neutral torus, and the solar wind. For in-situ observations of such ions, it is suitable to use ion energy mass spectrometers and magnetometers for space plasma observation missions such as Arase (Miyoshi et al., 2018) and BepiColombo/Mio (Milillo et al., 2020). Therefore, based on ion analyzer and magnetometer development experience gained from Kaguya (Yokota et al., 2005; Saito et al., 2008a; 2010; Tsunakawa et al., 2010), MMS (Pollock et al., 2016), ARASE (Yokota et al., 2017; Asamura et al., 2018; Matsuoka et al., 2018), and BepiColombo/MIO (Delcourt et al., 2009; 2016; Saito et al., 2020; Baumjohann et al., 2020), the Mass Spectrum Analyzer (MSA) will be composed of an ion energy mass spectrometer and magnetometers for the MMX mission. The MSA instrumentation is funded by the Japan Aerospace Exploration Agency (JAXA) and is being designed and developed in a collaboration of Osaka University and Kyoto University.

In this paper, we describe the goals of the MSA science investigation as well as document the conceptual design of the MSA instrumentation. In Sections 2 and 3, we describe the

MSA science goals in the context of the MMX mission and the MSA instrumentation, respectively. In Section 4, we present the expected observations by MSA in the Martian environment. Finally, we describe the current status of the MSA development and summarize the paper in Section 5.

2. Scientific objectives of MSA

Mars is the outermost terrestrial planet, close to the ice/water vapor sublimation boundary, the snowline, and is in the inner and outer solar system connection region along with the asteroid main belt. It is presumed that primordial small bodies around the snowline were supplied in large quantities to the terrestrial planetary regions and played a decisive role in the establishment of the surface life environment, including the crust, oceans and atmosphere (e.g., Maruyama & Ebisuzaki, 2017). Thus, the Martian moons may contain primordial materials and are key targets for investigating the material supply to the terrestrial planets (Kuramoto et al., this issue). The MMX mission is designed to accomplish two scientific major goals: 1) Clarify the origins of Martian moons and constrain processes for planetary formation and material transport in the region connecting the inner and outer solar system; and 2) From view point of the Martian moons, clarify the driving mechanism of the transition of the Mars-moon systems and add new knowledge to the evolution history of Mars. The two goals lead to the following six medium objectives: 1.1) Reveal whether Phobos originated as a captured asteroid or resulted from a giant impact; 1.2a) If Phobos is determined to be a captured asteroid, elucidate the composition and migration process of primitive materials supplied to the region of terrestrial planets and constrain the initial conditions of Martian surface evolution; 1.2b) If Phobos is determined to originate from a giant impact, elucidate giant impact and moon formation processes in the terrestrial planetary region and evaluate its influence on the early evolutionary process of Mars; 1.3) Place new constraints on Deimos' origin; 2.1) Obtain a basic description of the elementary processes of surface evolution for moons in the circum-Martian environment; 2.2) Add new findings and constraints on the history of changes in the Martian surface; and 2.3) Constrain the mechanisms of material circulation in the Martian atmosphere affecting the transitions in the Martian climate (for details, see Kuramoto et al., this issue). To accomplish the goals and objectives, the MMX mission will perform comprehensive remote-sensing and in-situ observations. In addition, more than 10-g Phobos materials will be collected and

delivered to Earth for detailed characterization using laboratory instrumentation (Usui et al., 2020). The MSA science investigation will address the MMX scientific goals which are related to in-situ ion and magnetic field observations in the Martian environment.

The MSA observations correspond to three of the six medium objectives 1.1, 2.1 and 2.2, as summarized in Table 1. Each medium objective is divided into different mission objectives (MOs). The MSA observations aim to accomplish the three medium objectives via four MOs, 1.1.1, 1.1.3, 2.1.1, and 2.2.2.

Table 1: MMX mission objectives corresponding to MSA observations.

Medium objectives	Mission objectives (MOs)	MSA observations
1.1 Reveal whether Phobos originated as a captured asteroid or resulted from a giant impact	1.1.1 Spectroscopically reveal the surface-layer distribution of the materials that make up Phobos with the spatial resolution required for the scientific evaluation of sampling points and geological structures, thereby constraining Phobos' origin.	1 Measure refractory ions (Si^+, Ca^+, Fe^+, etc.) emitted from the Phobos surface
	1.1.3 Obtain information such as molecular release rates and mass distribution related to the presence of ice in Phobos, investigate the presence or absence of density contrasts on Phobos' surface, and constrain Phobos' origin independently of MO1.1.1 and MO1.1.2.	2 Measure water-related ions (O^+, OH^+, H_2O^+ etc.) originating from inside Phobos (if they exist)
2.1 Obtain a basic description of the elementary processes of surface evolution for moons in the circum-Martian environment	2.1.1 Identify weathering and evolutionary processes (impact frequency, degree of gardening, and space weathering processes) in surface-layer regolith specific to the Martian moons as compared to asteroids	3 Measure incident ions to Phobos (H^+ and He^{++} of the solar wind and O^+ and O_2^+ etc. of the escaping ions from the Martian atmosphere), scattered ions, and emitted ions with monitoring the surrounding magnetic field
2.2 Add new findings and constraints on the history of changes in the Martian surface	2.2.2 Place constraints on the amount of atmospheric escape through the history of Mars from composition ratios and isotopic ratios in the current escaping atmosphere	4 Measure O^+, C^+, N^+, Ar^+ and some isotopes of them in the escaping ions from the Martian atmosphere

2.1 *Reveal whether Phobos originated as a captured asteroid or resulted from a giant impact (medium objective 1.1)*

The origin of the Mars moons is yet controversial, and two major theories have been proposed: primordial asteroid captures (e.g., Higuchi & Ida, 2017) and in-situ formation due to giant impacts (e.g., Rosenblatt et al. 2016). In the case of captured asteroid origin,

the Martian moons would preserve materials which had existed in the inner and/or outer solar system in early days. In the other case, the Martian moons would provide the second example of the giant impact following the Earth-Moon system and would substantially contain materials of the Martian origin. Therefore, either origin of the Martian moons revealed by the MMX mission will place constraints on not only the initial condition of the Mars-moons system but also the planet-forming processes and/or material transport in the connection region between the inner and outer solar system (Kuramoto et al., this issue).

Among the medium objective 1.1, MSA provides two observations which correspond to MO1.1.1: Spectroscopically reveal the surface-layer distribution of the materials that make up Phobos with the spatial resolution required for the scientific evaluation of sampling points and geological structures, thereby constraining Phobos' origin, and MO1.1.3: Obtain information such as molecular release rates and mass distribution related to the presence of ice in Phobos, investigate the presence or absence of density contrasts on Phobos' surface, and constrain Phobos' origin independently of MO1.1.1 and MO1.1.2. MSA will measure refractory ions emitted from the Phobos surface (MSA observation 1), and water-related ions originating from the inside Phobos (MSA observation 2), for MO1.1.1 and MO1.1.3, respectively (see Table 1).

2.1.1 *MSA observation 1: Refractory ions from Phobos surface*

The chemical composition of meteorites and returned samples provides various insights into the origin and evolution of their parent bodies (e.g, Saal et al., 2008, Terada et al., 2018). According to the database on the elemental abundance of meteorites, the composition ratios of several elements can be used to discriminate between different meteorite groups (Nittler et al., 2004). Thus, remote-sensing measurements of the chemical composition were made by orbiters equipped with X-ray and gamma-ray spectrometers in several solar system explorations (e.g., Feldman et al., 1998, Nittler et al., 2011, Lawrence et al., 2013), and are planned in the MMX mission using gamma-ray and neutron instruments (Lawrence et al., 2019).

When analyzing samples in the laboratory for the chemical composition, Secondary Ion Mass Spectrometry (SIMS) has been frequently used. In SIMS analysis, secondary ions are ejected from targeted samples by a primary ion beam and subsequently collected and analyzed by a mass spectrometer. In the case of small bodies which have no thick

atmosphere, the solar wind directly impacts their surface and sputters secondary ions, similarly to SIMS analysis. Fluxes of the secondary ions produced by solar wind sputtering are sufficiently large ($\geq \sim 10^4$ ions/cm^2 s) to be measured by standard spaceborne ion mass spectrometers (Elphic et al., 1991; Schaible, 2014; Duke & Baragiola, 2015). This means that ion observations by orbiters can be utilized for the SIMS analysis of small bodies (Johnson & Baragiola, 1991; Yokota & Saito, 2005). Lunar orbiters actually discovered such ions around the Moon (e.g., Yokota et al., 2009, Halekas et al., 2013). Because background sources of refractory ions are negligible, the measurement of such ions can be a robust method.

Since the density of the solar wind near Mars at ~1.5 Astronomical Unit (AU) is around half of that near the Earth and Moon, the total secondary ion flux from from Phobos is expected to be ~10^4 ions/cm^2 s assuming the ion emission is proportional to the solar wind flux. Estimates of the yield of secondary ions due to the solar wind and Martian magnetosphere ion sputtering are shown for a suite of Martian meteorite and carbonaceous chondrite compositions in Figure 1. Both the solar wind and plasma sheet ions eject significant fluxes of secondary ions. This is especially important due to the fact that Phobos is tidally locked to Mars so that the two hemispheres see distinctly different ion irradiation environments. The Mars-facing hemisphere is exposed to predominantly oxygen ions while the anti-Mars hemisphere is exposed to solar wind (Nenon et al., 2019), and thus distinguishing between magnetospheric oxygen and oxygen from water ice is critical. It was shown that classification of targeted small bodies can be carried out by measuring the flux ratios of refractory ions such as Mg^+, Ca^+, and Fe^+ to Si^+ even with an accuracy of ~50% (Schaible et al. 2017). Therefore, MSA measurements of secondary ions sputtered from Phobos by the solar wind (especially refractory ions) will allow us to discriminate between the formation models.

2.1.2 *MSA observation 2: Water-related ions from Phobos interiror*

To further constrain the origin of the Martian moons independently of observations of surface materials and analyses of returned samples, the MMX missions will examine their internal structures, especially the existence of ice. Captured primordial asteroids would preserve a large amount of ice inside them, while giant impacts cause depletion of volatile elements including water similarly to the Moon (e.g., Canap & Asphang, 2001). In the case of the captured asteroid origin, current H_2O release rate of ~0.3-3 g/s (~10^{22}-10^{23}

molecules/s) was calculated depending on the pore size and porosity by a model of the evolution of the water regime for Phobos (Fanale & Salvail, 1990). Re-accreted material would be volatile-depleted, but Phobos could still emit H_2O at a rate less than ~10^{20} molecules/s, assuming that all oxygen is released as H_2O. This water could be caused/supplied by reactions of solar wind hydrogen with refractory oxygen in the surface rocks, escaping ions from the Martian atmosphere, and micrometeoroid impact (Chipriani et al., 2011; Poppe & Curry, 2014), Therefore, H_2O flux of ~10^{22} molecules /s is an indicator of the presence or absence of ice in Phobos.

Released H_2O molecules can easily escape the orbit of Phobos, and become trapped in a keplerian orbit around Mars (Ip and Banaszkiewicz, 1990), forming an envelope of all the permitted trajectories, or 'torus' (Krymskii et al., 1992). Peak densities of 10^4-10^5 molecules/cm^3 were derived from a model of the H_2O-related molecular gas torus (Mura et al., 2002) using the release rate of 10^{23} molecules /s. In the Phobos-2 observation, electromagnetic ion beam waves were observed, implying the existence of a Phobos neutral gas torus (Baumgärtel et al., 1998). On the other hand, during the solar minimum, no signatures related with such a Phobos torus were observed by Mars Express (Futaana et al., 2010a) and Mars Global Surveyor (Øieroset et al., 2010).

The existence of ice in Phobos is expected to results in the H_2O emission of ~10^{22}-10^{23} molecules/s and formation of the H_2O gas torus of 10^4-10^5 molecules/cm^3 (Mura et al., 2002). In the case of the H_2O emission rate of 10^{22} molecules /s, the peak flux of H_2O-related ions (O^+, OH^+, H_2O^+, etc) of ~10^7 ions/cm^2 s can be estimated (Poppe & Curry, 2014). Such ion fluxes can be observed by standard spaceborne ion energy mass analyzers designed for measuring ions of 10^4-10^8 ions/cm^2 s in the solar wind and planetary magnetosphere (e.g., Yokota et al. 2005; 2017). Therefore, the observation of such ions by MSA can determine whether the Phobos contains large amount of ice and whether its origin is a captured primordial asteroid or in-situ formation by a giant impact.

2.2 *Obtain a basic description of the elementary processes of surface evolution for moons in the circum-Martian environment (medium objective 2.1)*

The surfaces of small bodies experience changes in their chemical composition and reflection spectrum, called 'space weathering' (Chapman, 2004), caused by the impact of micrometeoroids (Sasaki et al., 2001) and solar wind ions (Vernazza et al., 2009, Matsumoto et al., 2020). The presence of planet Mars affects the frequency and velocity

237 of meteorite and micrometeoroid impacts onto the Martian moons, and escaping ions
238 from the Martian atmosphere as well as solar wind ions collide with their surfaces (Nenon
239 et al., 2019). The nearside of Phobos, the rotation of which is currently synchronized with
240 its revolution, might contain much more particles from the Martian atmosphere.
241 Therefore, the space weathering of the Martian moons is probably different from that of
242 other moons and asteroids in the main belt.
243 To achieve medium objective 2.1, the MMX mission has the following task, MO2.1.1:
244 Identify weathering and evolutionary processes (impact frequency, degree of gardening,
245 and space weathering processes) in surface-layer regolith specific to the Martian moons
246 as compared to asteroids. To address MO2.1.1, MSA has observation 3: Measure incident
247 ions to Phobos, scattered ions, and emitted ions while monitoring the surrounding
248 magnetic field (see Table 1).
249 The solar wind typically has a flux of ~10^8 particles/cm^2 s composed of ions (mostly H^+
250 and He^{++}) and electrons, sometimes varying from 10^{-1} to 10 times, with a magnetic field
251 of ~1~10s nT around Mars (Trotignon et al., 1996). When the Martian moons are
252 downstream of the solar wind relative to Mars, they are substantially shielded from the
253 solar wind ions, but are exposed to escaping ions from the Martian atmosphere (O^+, O_2^+,
254 etc.) of ~10^4~10^7 ions/cm^2 s (e.g., Lundin et al., 2004; Dong et al., 2015; Ramstad et al.,
255 2017). In the case of the Earth's Moon, ~0.1~1% of incident solar wind protons are back
256 scattered as still protons (Saito et al., 2008b), ~20% as neutral hydrogen atoms (McComas
257 et al., 2009, Wieser et al., 2009), while the rest is probably injected into the lunar surface.
258 The back scattering of the solar wind was also observed around Phobos (Futaana et al.
259 2010a). The solar wind not only bombards the dayside surface of the Moon but also
260 intrudes the wake region because of electromagnetic effects (Futaana et al., 2010b;
261 Nishino et al., 2009, 2010, 2013; Dhanya et al., 2017). In addition, some of the solar wind
262 is reflected in the Earth's bow shock and irradiate the nightside of the Moon (Nishino et
263 al., 2017).
264 Since the Moon has large and wide magnetic anomalies (e.g., Richmond & Hood, 2008,
265 Tsunakawa et al., 2015), which deflect and/or reflect the solar wind (Saito et al., 2012),
266 some areas are substantially shielded from the solar wind by an induced electric field
267 (Futaana et al., 2013). Such a shielding from the solar wind can reduce the progression of
268 the space weathering (Kramer et al., 2011, Bamford et al., 2016). Although there is no
269 unambiguous evidence for the existence of magnetic anomalies on Phobos (Mordovskaya

2001; Veselovsky, 2004), their electromagnetic effects have a significant influence on the space weathering if exist.

As described in Section 2.1.1, secondary ions are emitted by the solar wind sputtering that affects evolutionary processes of the surface regolith layer. The ion emissions for various species were estimated at ~10^4 /cm^2 s around Phobos (Poppe & Curry, 2014). In the case of the Earth's Moon, secondary ion emissions of ~10^4 ions/cm^2 s were estimated (Yokota and Saito, 2005) and were actually observed (e.g., Yokota et al., 2009, Tanaka et al., 2009) for a variety of ions, preferably volatile species (Yokota et al., 2014, 2020). To reveal how much ions go toward and come from the Martian moons for each ion species, MSA will measure solar wind ions (mostly H^+ and He^{++}), escaping ions from the Martian atmosphere (O^+, O_2^+, etc.), back-scattered solar wind ions, and secondary ions emitted from the Martian moons. In addition, MSA will also measure a magnetic field to investigate the surrounding electromagnetic effects and to search magnetic anomalies on the Martian moons.

2.3 *Add new findings and constraints on the history of changes in the Martian surface (medium objective 2.2)*

The Martian moons would contain substantial materials of the Martian origin which have carried since their birth via ejecta (Hyodo et al., 2019) and escaping ions (e.g., Inui et al., 2018, Nénon, et al., 2019). The heavy isotope enrichment in major elements (C, O, etc.) in the lower Martian atmosphere measured by the Curiosity rover supported the hypothesis of substantial atmospheric escape (Mahaffy et al., 2013). Thus, in the MMX mission, the information on the history of the Mars surface environment evolution can be provided by the analysis of returned samples (Usui et al., 2020). In addition, the MSA ion observations will evaluate not only the current status of the Martian atmospheric escape but also will constrain its history using the isotope ratios (e.g., Jakosky et al., 2017). To contribute to the accomplishment of medium objective 2.2, MSA has observation 4: Measure O^+, C^+, N^+, Ar^+ and some isotopes of them in the escaping ions from the Martian atmosphere, which corresponds to one of the mission objectives, MO2.2.2: Place constraints on the amount of atmospheric escape through the history of Mars from composition ratios and isotopic ratios in the current escaping atmosphere (see Table 1).

In the escape processes of the Martian atmosphere, the lighter species are preferentially removed, resulting into a remaining atmosphere enriched in the heavier isotopes (e.g.,

McElroy & Yung, 1976, Chassefiere & Leblanc 2004). Ignoring the supply and loss of materials other than atmospheric escape, such as exchange with the surface and crust, the amount of the Martian atmosphere $N(t)$ for each species at time t is expressed by a simplified equation (Chassefiere & Leblanc 2004):

$$N(t) = N_0 r(t)^{1/(f-1)},$$

where N_0, $r(t)$, and f indicate the initial amount, isotope abundance ratio at normalized by the initial one, and isotope fractionation factor, respectively. To estimate $r(t)$, the current and initial isotope abundance ratios in the Martian atmosphere are derived from the observation data by the Curiosity rover and the analysis of primordial chondrites, respectively. Because f is determined by the isotope abundance ratio at the exobase, the MAVEN observation estimated f for $^{38}Ar/^{36}Ar$ and then calculated N_0, suggesting that 66% of the atmospheric argon has been lost to space (Jakosky et al., 2017). In the MMX mission, f for $^{18}O/^{16}O$, $^{13}C/^{12}C$, etc. will be derived from the MSA observation of escaping atmospheric ions.

Previous observations and computations using a model of the upper atmosphere estimated f, while the estimate had a large (~400%) variation for $^{18}O/^{16}O$ (e.g., McElroy & Yung, 1976; Fox and Hac, 2010). Thus, the estimate of f within a 50% accuracy is needed in the MMX mission for further constraints on the total loss amounts of the Martian atmosphere.

3. Instrumentation of MSA

The MSA instrument is composed of an ion energy mass spectrometer, two magnetometers, and electronics (see Fig. 2). The ion analyzer measures distribution functions and mass distributions of low-energy (<~10s keV) ions. The magnetometers measure the magnetic field of the solar wind which is sometimes perturbed by Mars and possibly by Phobos. The combination of ion and magnetic field sensors will allow us to measure ions emitted from Phobos and its torus as well as escaping ions from the Martian atmosphere with monitoring the solar wind to address the MMX science goals.

3.1 *MSA ion energy mass spectrometer*

The MSA ion energy mass spectrometer employs nearly the same measurement techniques as that of Ion energy Mass Analyzer (IMA) for the Kaguya mission (Yokota et al., 2005; Saito et al., 2008a, 2010) and Mass Spectrum Analyzer (MSA) for

BepiColombo/MIO (Delcourt et al., 2009, 2016; Saito et al., 2020). Figure 3 shows a cross section of an engineering model of the MSA ion energy mass analyzer. The ion analyzer cylindrically symmetric in shape and consists of an energy analyzer and a mass analyzer. The aperture of 360° near the sensor top and neighboring angular scanning deflectors provide a $\sim 2\pi$ steradian field-of-view (FOV) (Yokota et al., 2005). The two angular scanning deflectors are alternately applied with a sweeping high voltage up to +5 kV for such a wide FOV. The energy analyzer measures energy/charge E/q using a top-hat electrostatic method (e.g., Carlson et al., 1982) in which the inner-spherical electrode is applied with a sweeping negative high voltage. In the mass analyzer, mass/charge m/q is measured by a time-of-flight (TOF) method, that use a linear-electric field (LEF) for the higher mass resolution (e.g., McComas &Nordholt, 1990). At the entrance of the mass analyzer, ultra-thin carbon foil is mounted on a metal grid to emit secondary electrons for start signals. The TOF chamber is longer than that of the previous analyzers and is optimized to achieve a high mass resolution ($m/\Delta m > 100$) (Gilbert et al., 2010). Both ends of the TOF chamber is supplied with static high voltage up to $\pm\sim 12$ kV for a post acceleration and reflection of incident ions, respectively. The incident ions are detected by a micro-channel plate (MCP) assembly at the bottom as stop signals if they are neutralized by the carbon foil. In the other case, the incident ions pass through the carbon foil as ions and then are reflected by the LEF, resulting in ejection of secondary electrons at the ceiling of the TOF chamber. The secondary electrons are attracted by the LEF and are also detected by the MCP assembly as stop signals. The MCP assembly has a circular delay line anode to obtain the start signal and 360°-position information from the detection of the secondary electrons emitted from the carbon foil (Saito et al., 2017). The specifications of the MSA ion analyzer are listed in Table 2.

Table 2: Specifications of the MSA ion energy mass spectrometer.

Parameters	Value	Notes
Energy range	~5 -~30k eV/q	
resolution	~10%	$\Delta E/E$ (FWHM)
FOV range	$\geq 2\pi$ sr	
resolution	22.5° ×12.25° per channel	FWHM
Mass range	1-100 amu	
resolution	> 100	$m/\Delta m$ (FWHM)
Geometric factor	$\geq 10^4$ cm^2 sr eV/eV per channel	Calculated in the numerical model

3.2 *MSA Magnetometer*

Fundamental mode orthogonal fluxgate (FM-OFG) technique is used for the two magnetometers which are the components of MSA. FM-OFG was firstly proposed by Sasada (2002) and successively 'bias switching' method of the sensor excitation was designated to drastically reduce the offset in the output signal (Sasada and Usui, 2003, Koga and Sasada, 2003). Recently the sensor and circuit design to apply FM-OFG to the space missions has been developed by improving the offset stability and noise characteristics (Murata et al., 2018, Murata et al., 2019). FM-OFG technique achieves significantly down-sized and lightened sensor in comparison with the conventional parallel fluxgate magnetometers which have been generally used for the space missions. FM-OFG is much effective to reduce the power to excite the sensor as well.

Each of two MSA magnetometers measures three orthogonal components of the magnetic field. Figure 4 shows the schematic configuration of the magnetometer with a single sensor head, while the actual sensor unit has three heads whose axes are arranged orthogonally. In the sensor head part, a couple of amorphous wire cores are strained in parallel along a resin bobbin of rod shape. The tips of the cores are connected through the copper bonding, and the roots are connected to the excitation circuit in the electronics part implemented in the MSA electronics box. The excitation circuit directly apply the DC-biased AC excitation current, which is sinusoidal AC (f=74kHz) current superposed on DC (bias) current, to the core. The polarity of the excitation current is periodically flipped (bias switching). The signal of same f Hz induced in the pickup coil wound around the bobbin is detected by the electronics part. More details about the FM-OFG technique using bias switching are described in Murata et al. (2018) and Murata et al. (2019). The specifications of the MSA magnetometer are listed in Table 3.

Table 3: Specifications of the MSA magnetometers.

Parameters	Value	Notes
Dynamic range	±8000nT / ±60000nT	Switched by command
Resolution	0.1 nT / 0.8 nT	
Sampling rate	1 Hz	Nominal observation
	128 Hz	Checkout mode
Noise level	< 15 pT/$\sqrt{\text{Hz}}$	at 1 Hz
Offset stability	< 0.027 nT/°C	

3.3 MSA electronics box

The MSA instrument include an electronics box which is installed inside the spacecraft

structure. Each analog signal from the MSA ion analyzer and magnetometers is collected by the electronics box via each pre-amplifier (see Figure 2). The signal processing and data allocation for the ion analyzer and magnetometers are made by an FPGA with CPU cores. The FPGA also monitors and controls High Voltage Power Supplies (HVPSs) that are mounted near the ion analyzer. Telemetry commands and data are transmitted and are received via the space wire interface to the spacecraft system. The electronics box as a DC-DC converter to provide ± 12 V, +5 V, and +3.3V to each electronic board.

4. Estimation of future observation

The MSA ion spectrometer employs the techniques used for previous ion analyzers for space plasma observation which measured from solar wind ions of ~10^8 ions/cm^2 s to planetary magnetospheric ions of $\geq \sim 10^4$ ions/cm^2 s. Thus, MSA has sufficient performance to measure secondary ions of ~10^4 ions/cm^2 s from Phobos (MSA observation 1), water-related ions of ~10^7 ions/cm^2 s originating from the Phobos torus if exists (MSA observation 2), solar wind ions of ~10^8 ions/cm^2 s and those scattered at the Phobos surface of 10^5~10^6 ions/cm^2 s (MSA observation 3), and escaping ions from the Martian atmosphere of ~10^4~10^7 ions/cm^2 s (MSA observation 4). Compared to previous ion analyzers for the Mars missions (e.g., Barabash et al., 2004; Wilson, 2004; McFadden et al., 2015), only the mass resolution will be improved to $M/\Delta M \geq$~100 to clearly discriminate heavy ions and their isotope from each other. Therefore, successful investigations by MSA mainly depend on the configuration and period of the observation.

4.1 *MSA ion observation*

During the nominal scientific observation period, the MMX spacecraft will be in a quasi-satellite orbit, orbiting Mars together with Phobos at a distance of ~20~200 km from each other (Nakamura et al., this issue). Figures 5A and 5B show the MSA observation configurations, focusing on the relations with Phobos/Mars in the Phobos/Mars-centric Solar Ecliptic coordinates, respectively. The Phobos/Mars-centric Solar Ecliptic coordinate system has the X-axis pointing from Phobos/Mars towards the Sun, the Z-axis parallel to the ecliptic northern pole, and the Y-axis determined in the right-handed system. When the spacecraft is in the neighboring of Phobos, the hemispherical FOV of MSA can capture both solar wind ions and those scattered at the Phobos surface in most situations. Because the spacecraft orbits along to the Martian torus, water-related ions

generated from the torus are easily observed if such a gas torus exists. The observations of water-related ions are suitable in the dayside of Mars because it is straightforward to distinguish between ions from the torus and those from the Martian atmosphere. When the spacecraft and Phobos are behind Mars with respect to the Sun at an interval of 7.66 hours, there is an opportunity to observe escaping ions from the Martian atmosphere.

The motion of charged particles is determined by the surrounding electric and magnetic fields ($\boldsymbol{E}$ and $\boldsymbol{B}$) in space. The equation of motion in $\boldsymbol{E}$ and $\boldsymbol{B}$ is expressed as $m\dot{\boldsymbol{v}} = q(\boldsymbol{E} + \boldsymbol{v} \times \boldsymbol{B})$, where m, q, and $\boldsymbol{v}$ denote the mass, charge, and velocity of the charged particle, respectively. Thus, the information of $\boldsymbol{E}$ and $\boldsymbol{B}$ is indispensable for an adequate interpretation of the ion behavior measured by MSA. In the Martian environment, the solar wind electric and magnetic fields are dominant upstream from Mars, while the shocked and tail regions are formed downstream. In the solar wind, MSA can derive both $\boldsymbol{B}$ and $\boldsymbol{E}$ from its measurements, because the solar wind electric field is given by $\boldsymbol{E} = -\boldsymbol{V} \times \boldsymbol{B}$, where $\boldsymbol{V}$ indicates the solar wind velocity measured by the MSA ion analyzer.

As a reference for the ion observations around Phobos, the observation results around the Moon can be used, obtained by IMA on the Kaguya spacecraft (Saito et al., 2010) (see Figure 6). The energy-time spectrogram obtained by IMA shows that solar wind ions, those scattered at the lunar surface and reflected by the lunar magnetic anomalies, and secondary ions emitted from the Moon were measured in a couple of hours. Since the spacecraft was nadir-pointing, IMA measured solar wind ions only around the pole regions, while those scattered at the lunar surface were measured over the dayside surface. Although the scattered solar wind ions lose ~50% of their incident energies, they travel against the solar wind for a short distance (~100s km) (Saito et al., 2008b). Thus, the scattered solar wind ions can be measured around Phobos when the distance is less than ~100s km. On the other hand, the initial energies of secondary ions sputtered by the solar wind are mostly less than a couple of electron volts (Madey et al., 1998 and references therein). Consequently, secondary ions move in a straight direction along $\boldsymbol{E}$ over a short distance (~100s km) compared to their Larmor radii (100s—1000s km), while they are in a pickup ion motion due to the solar wind (Yokota & Saito, 2005). The motion of the ions generated in the torus is almost the same as that of the secondary ions from Phobos, because their energies in the torus gas before photoionization are less than a few electron volts. Their measured energies κ are determined by $\kappa = L|\boldsymbol{E}|$, where L indicates the

458 distance between the emission/ionization points of the ions and spacecraft positions (see
459 Figure 5A).
460 Different from the observations of the solar wind ions and those scattered at the surface,
461 the observation of pickup ions generated from the torus and Phobos considerably depends
462 on $\boldsymbol{E}$. Since the torus is widely distributed and is continuously tracked by the spacecraft,
463 MSA has many opportunities to observe ions from the torus. However, the observation
464 of secondary ions emitted from Phobos with a diameter of $d{\sim}22.5$ km (MSA
465 observation 1) are comparatively limited. A requirement of the MSA observation 1 is that
466 the positions of the spacecraft and Phobos are in the same plane whose normal vector is
467 parallel to $\boldsymbol{V}$ (see Figure 7). In other words, the spacecraft is in the YZ plane in the
468 Phobos-centric Solar Ecliptic coordinates because $\boldsymbol{V}$ is approximately on the -X axis.
469 During the nominal observation, the spacecraft will periodically stay in the dayside and
470 nightside of Phobos and thus will path through the YZ plane many times (Nakamura et
471 al., this issue). In addition, MSA observation 1 has another requirement that $\boldsymbol{E}$ directs
472 from Phobos to the spacecraft. Assuming the direction of $\boldsymbol{B}$ is non-biased, the possibility
473 is approximately given by $d/2\pi L$ for spacecraft in the YZ plane, where d and L
474 denote the diameter of Phobos and spacecraft's altitude, respectively. Although high-
475 altitude (~100 km) observations provide the possibility below 5 %, the observation period
476 for secondary ions from Phobos will be secured by low-altitude (10—30 km)
477 observations with the possibility of 10s %.
478 It should be noted that if Phobos had large and wide-area magnetic anomalies sufficiently
479 to capture secondary ions, MSA would measure no ions from Phobos. In the case of the
480 Earth's Moon, Kaguya observed solar wind ions reflected from magnetic anomalies
481 rather than secondary ions from the lunar surface (see Figure 6). In such an extreme case,
482 the MSA magnetometer would tell us what disturbs the MSA ion observation.
483
484 4.2 *MSA magnetic field observation*
485 As described in the previous subsection, magnetic field vector $\boldsymbol{B}$ is indispensable to
486 interpret the ion behavior measured by the MSA ion energy mass spectrometer. The MSA
487 magnetometer is required to measure the magnetic field strength and direction with good
488 accuracy.
489 The magnetic field strength in the solar wind at the Mars orbit is typically 3 nT although
490 it significantly varies depending on the condition of the solar surface. Disturbing fields

491 from other components on the spacecraft would cause problems to determine the strength
492 and direction of such weak magnetic field. In the previous missions measuring weak
493 magnetic field in the space, very often the magnetometer sensors have been mounted at
494 the tips of the long booms to avoid the disturbances. In the case of MMX where boom is
495 not available, however, the disturbing noises are planned to be identified quantitatively
496 by analyzing the output values from two magnetometers. At two apart measurement
497 positions on the surface of the spacecraft, the artificial magnetic fields caused by the
498 onboard components have different intensity and direction, while the natural magnetic
499 fields are same. The magnetic field data are able to be 'cleaned' by analyzing the
500 difference between the fields measured by two magnetometers. Similar method has been
501 used in the missions where it is difficult to implement boom for magnetometer or carry
502 magnetic cleanliness of the spacecraft (Georgescu et al., 2008, Pope et al., 2011,
503 Constantinescu et al., 2020).
504 In the orbit, the MSA magnetometer produces the magnetic field data with 1 Hz sampling
505 rate. Besides, it has 128 Hz sampling mode for the instrument checkout. It is much
506 desirable to operate the MSA magnetometer during the cruising to Mars for the purposes
507 of the instrument health check as well as for the scientific study of the interplanetary
508 plasma physics.
509 The MSA magnetometer will be operated basically together with the MSA ion energy
510 mass spectrometer. On the other hand, even without the data from the ion energy mass
511 spectrometer, it is much valuable to measure the magnetic fields, especially at the landing
512 operation to Phobos. The intrinsic and crustal magnetic fields of Phobos are essential to
513 interpret the interior structure and surface composition. Although there is no reliable
514 information for deriving the magnetic moment of Phobos so far (Veselovsky, 2004),
515 Mordovskaya et al. (2001) estimated the magnetic field intensity at the Phobos surface to
516 be 0.6G (same intensity as geomagnetic surface field) from the magnetopause position
517 identified by Phobos-2. Even less intense, it is possible that magnetic moments could be
518 detected if the magnetic fields originated from the ancient Mars magnetized Phobos as
519 well as the Martian slab. Sprenke and Baker (2000) identified the moment density of the
520 Martian magnetized slab as 10 A/m. Because the intensity of the magnetic field is
521 proportional to $1/r^3$, where r denotes the distance, the moment density of Phobos is
522 0.4 A/m assuming the magnetization occurs proportionally to the applied field intensity.
523 In our estimation where Phobos is a sphere with a radius of 10 km radius homogeneously

magnetized at 0.4 A/m, the magnetic field intensity is more than 3 nT, the typical intensity of the magnetic field in the solar wind at the Martian orbit, at distances shorter than 30 km from the surface. The magnetic field, if detected, would give important insights into the global magnetism of Mars and its history.

The time variation of the magnetic field originating from the Phobos interior can be an indicator of the electrical current flowing under the surface induced by the variation in the external magnetic field. Observations of the time variation would allow us to estimate the electrical conductivity of the material from the surface to the skin depth, and thus provide important information about the crustal material and its condition. Similar observations were carried out by the Apollo Moon missions, and is planned in the Jupiter JUICE mission to investigate a subsurface ocean (Grasset et al., 2013).

5. Summary

The preliminary design phase for MSA was completed in Octorber 2020. The development of an engineering model of the MSA instrument has initiated, aiming the final delivery in 2023 and launch of the MMX spacecraft in 2024. To address the MMX mission goals, MSA will perform in-situ observations of ions and magnetic field, which are related with the surface and tori of the Martian moons, and Martian atmosphere, and the solar wind. In addition, MSA will also participate in a joint Mars observation program which is currently being defined (e.g., Ogohara et al., this issue).

Declarations

The authors *must* provide the following sections under the heading "Declarations".

Ethics approval and consent to participate

Not applicable

Consent for publication

Not applicable

List of abbreviations

AU: Astronomical Unit

FM-OFG: Fundamental mode orthogonal fluxgate
FOV: Field-Of-View
HVPS: High Voltage Power Supply
IMA: Ion Mass Analyzer
JAXA: Japan Aerospace Exploration Agency
LEF: Linear-Electric Field
MCP: Micro-Cannel Plate
MMX: Martian Moons eXploration
MO: Mission Objective
MSA: Mass Spectrum Analyzer
SIMS: Secondary Ion Mass Spectrometry
TOF: Time-Of-Flight

Availability of data and materials

The data and materials used in this research are available on request to the corresponding author, Dr. Shoichiro Yokota (yokota@ess.sci.osaka-u.ac.jp).

Competing interests

The authors declare that they have no competing interests.

Funding

This research was partially supported by a Grant-in-Aid for Scientific Research from the Japan Society for the Promotion of Science (# 20K04039, #17H01164, #17H02970).

Authors' contributions

SY, NT, AM, NM, and MJS wrote the manuscript. SY, YS, DD, KA, and SK contributed to the development of the ion analyzer. AM, NM, and RM contributed to the development of the magnetometer. NT, KS, YF, HN, MNN, KK, and YH contributed to consideration of the observation objectives. SI contributed to the magnetic field data analysis plan.

Acknowledgements

The authors would like to express sincere thanks to all members of the MMX mission for their supports. The MSA components are now being

manufactured by Meisei Electric Co., Ltd. The ion optics is machined by YS design. The magnetometer sensors are now being manufactured by Tierra Tecnica Ltd.

Authors' information

Endnotes

References

Agee CB et al. (2013) Unique meteorite from early Amazonian Mars: water-rich basaltic breccia Northwest Africa 7034, Science 339, 780–785 doi:10.1126/science.1228858

Albee AL, Arvidson RE, Palluconi F, Thorpe T (2001) Overview of the Mars Global Surveyor mission, J. Geophys. Res.: Planets, 106(E10), 23291—23316, doi.org/10.1029/2000JE001306

Asamura K, Kazama Y, Yokota S, Kasahara S, Miyoshi Y (2018) Low-energy particle experiments - ion analyzer (LEPi) onboard the ERG (Arase) satellite, Earth Planets Space, 70:70. doi.org/10.1186/s40623-018-0846-0

Barabash S et al. (2004) ASPERA-3: Analyser of Space Plasmas and Energetic Ions for Mars Express, in Mars Express: The Scientific Payload, A. Wilson, Ed. (ESA Special Publication SP-1240, 2004), pp. 121–139.

Barabash S, Fedorov A, Lundin R, Sauvaud J-A (2007) Martian atmospheric erosion rates. Science 315, 501–503. doi:10.1126/science.1134358

Baumgärtel K, Sauer K, Dubinin E, Tarrasov V, Dougherty M (1998) “Phobos events”—Signatures of solar wind interaction with a gas torus? Earth Planets Space, 50, 453–462,

619 Baumjohann W, et al. (2020) The BepiColombo–Mio Magnetometer en Route to
620 Mercury. Space Science Reviews, 216(8), 125.
621
622 Bamford RA et al (2016) 3D PIC simulations of collisionless shocks at lunar magnetic
623 anomalies and their role in forming lunar swirls. Astrophys. J. 830, 146.
624 doi.org/10.3847/0004-637X/830/2/146
625
626 Borg LE et al. (2005) Constraints on the U-Pb isotopic systematics ofMars inferred
627 from a combined U-Pb, Rb-Sr, and Sm-Nd isotopic study of theMartian meteorite
628 Zagami. Geochim. Cosmochim. Acta 69, 5819–5830 doi:10.1016/j.gca.2005.08.007
629
630 Canup RM, Asphang E (2001) Origin of the Moon in a giant impact near the end of the
631 Earth's formation. Nature 412, 708–712.
632
633 Carlson CW, Curtis DW, Paschmann G, Michel W (1982) An instrument for rapidly
634 measuring plasma distribution functions with high resolution. Adv Sp Res 2(7):67–70
635
636 Chapman, CR, (2004) Space weathering of asteroid surfaces, Ann. Rev. Earth Planet.
637 Sci. 32, 539-567 doi.org/10.1146/annurev.earth.32.101802.120453
638
639 Chassefiere E, Leblanc F (2004) Mars atmospheric escape and evolution; interaction
640 with the solar wind, Planetary and Space Science 52(11):1039-1058
641 doi.org/10.1016/j.pss.2004.07.002
642
643 Cipriani F, Witasse O, Leblanc F, Modolo R, Johnson RE (2011) A model of interaction
644 of Phobos' surface with the martian environment, Icarus 212(2), 643-648
645 doi.org/10.1016/j.icarus.2011.01.036
646
647 Constantinescu OD et al. (2020) Principal Component Gradiometer technique for
648 removal of spacecraft-generated disturbances from magnetic field data. Geosci. Instrum.
649 Method. Data Syst. Discuss. 2020, 1-26.
650
651 Delcourt D, et al. (2009) The mass spectrum analyzer (MSA) onboard BEPI

652 COLOMBO MMO: Scientific objectives and prototype results, Advances in Space Res.
653 43 869–874, 2009. doi.org/10.1016/j.asr.2008.12.002
654
655 Delcourt D, et al. (2016) The Mass Spectrum Analyzer (MSA) on board the
656 BepiColombo MMO J. Geophys. Res.-Space Physics 121(7) 6749-6762
657
658 Dhanya MB, Bhardwaj A, Futaana Y, Barabash S, Wieser M, Holmström M, Wurz P
659 (2017) New suprathermal proton population around the moon: Observation by SARA
660 on chandrayaan-1. Geophys. Res. Lett., 44 (10):4540–4548, 2017. doi:
661 10.1002/2017GL072605. URL
662
663 Dong, Y., et al. (2015) Strong plume fluxes at Mars observed by MAVEN: An
664 important planetary ion escape channel, Geophys. Res. Lett., 42(21), 8942-8950
665 doi.org/10.1002/2015GL065346
666
667 Dukes, CA, Baragiola, RA (2015) The lunar surface‐exosphere connection:
668 Measurement of secondary‐ions from Apollo soils. Icarus 255, 51-57.
669 doi.org/10.1016/j.icarus.2014.11.032
670
671 Elphic RC, Funsten III. HO, Barraclough BL, McComas DJ, Paffett MT, Vaniman DT,
672 Heiken G (1991) Lunar surface composition and solar wind-induced secondary ion
673 mass spectrometry. Geophys. Res. Lett. 11, 2165–2168.
674
675 Fanale FP, Salvail JR (1990) Evolution of the water regime of Phobos, Icarus,
676 88(2):380-395, doi.org/10.1016/0019-1035(90)90089-R
677
678 Fox JL, Hac A (2010) Isotope fractionation in the photochemical escape of O from
679 Mars, Icarus 208, 176–191 doi.org/10.1016/j.icarus.2010.01.019
680
681 Fujiwara A et al. (2006) The rubble-pile asteroid Itokawa as observed by Hayabusa.
682 Science 312, 1330–1334
683
684 Futaana Y, Barabash S, Holmström M, Fedorov A, Nilsson H, Lundin R, Dubinin E,

685 Fränz M (2010a) Backscattered solar wind protons by Phobos, J. Geophys. Res.,
686 115:A10213, doi.org/10.1029/2010JA015486
687
688 Futaana Y et al. (2010b) Protons in the near-lunar wake observed by the Sub-keV Atom
689 Reflection Analyzer on board Chandrayaan-1. J. Geophys. Res., 115(A10) 10
690 doi.org/10.1029/2010JA015264.
691
692 Futaana Y et al. (2013) Remote energetic neutral atom imaging of electric potential over
693 a lunar magnetic anomaly, 40(2), Geophysical Research Letters, 262-266
694 doi.org/10.1002/grl.50135
695
696 Georgescu E, et al. (2008) Modified gradiometer technique applied to Double Star (TC-
697 1). Advances in Space Research, 41(10), 1579-1584.
698
699 Gilbert JA, Lundgren RA, Panning MH, Rogacki S, Zurbuchen TH (2010) An
700 optimized three-dimensional linear-electric-field time-of-flight analyzer, Review of
701 Scientific Instruments, 81(5) 053302 doi.org/10.1063/1.3429941
702
703 Grasset O et al. (2013) JUpiter ICy moons Explorer (JUICE): An ESA mission to orbit
704 Ganymede and to characterise the Jupiter system, Planetary and Space Science, 78, 1-
705 21.
706
707 Grotzinger JP et al. (2012) Mars Science Laboratory Mission and Science Investigation,
708 Space Sci. Rev. 170, 5–56 doi.org/10.1007/s11214-012-9892-2
709
710 Halekas S, Poppe AR, Delory GT, Sarantos M, McFadden JP (2013) Using ARTEMIS
711 pickup ion observations to place constraints on the lunar atmosphere. J. Geophys. Res.
712 Planets 118, 81–88 doi.org/10.1029/2012JE004292
713
714 Higuchi A, Ida S (2017) Temporary capture of asteroids by an eccentric planet.
715 Astrophys. J. 153, 155
716
717 Hyodo R et al. (2019) Transport of impact ejecta from Mars to its moons as a means to

718 reveal Martian history. Sci. Rep. 9, 19833 doi.org/10.1038/s41598-019-56139-x
719
720 Inui S et al. (2018) Cold dense ion outflow observed in the Martian ‐ induced
721 magnetotail by MAVEN. Geophysical Research Letters, 45, 5283– 5289.
722 doi.org/10.1029/2018GL077584
723
724 Ip WH, Banaszkiewicz M (1990) On the dust/gas tori of Phobos and Deimos Geophys.
725 Res. Lett., 17 857-860 10.1029/GL017i006p00857
726
727 Jakosky BM et al. (2015) The Mars Atmosphere and Volatile Evolution (MAVEN)
728 Mission, Space Sci. Rev. 195, 3–48. doi.org/10.1007/s11214-015-0139-x
729
730 Jakosky BM et al. (2017) Mars' atmospheric history derived from upper-atmosphere
731 measurements of 38Ar/36Ar, Science, 355(6332), 1408-1410
732 doi.org/10.1126/science.aai7721
733
734 Johnson R, Baragiola R (1991). Lunar surface: Sputtering and secondary ion mass
735 spectrometry. Geophysics Research Letters, 18(11), 2169–2172.
736 https://doi.org/10.1029/91GL02095
737
738 Koga F and Sasada I (2003) Low offset orthogonal fuxgate operating in fundamental
739 mode. Journal of the Magnetics Society of Japan, 27, 410-413.
740
741 Kramer GY (2011) Characterization of lunar swirls at Mare Ingenii: A model for space
742 weathering at magnetic anomalies, J. Geophys. Res. Planets, 116, E4
743 doi.org/10.1029/2010JE003669
744
745 Krymskii AM, Breus TK, Dougherty MK, Southwood DJ, and Axford WI (1992) The
746 electromagnetic effects of the solar wind interaction with the Phobos neutral gas halo
747 and dust torus, Planet. Space Sci., 40(8), 1033, 1992. doi.org/10.1016/0032-
748 0633(92)90032-J
749
750 Kuramoto K et al., Martian Moons Exploration MMX: Sample Return Mission to

751 Phobos Elucidating Formation Processes of Habitable Planets, this issue
752
753 Lammer H, Lichtenegger HIM, Kolb C, Ribas I, Guinan EF, Abart R, Bauer SJ, (2003)
754 Loss of water from Mars: Implications for the oxidation of the soil, Icarus, 165(1), 9-25
755 doi.org/10.1016/S0019-1035(03)00170-2
756
757 Lawrence DJ et al. (2013) Evidence for water ice near Mercury's north pole from
758 MESSENGER Neutron Spectrometer measurements. Science, 339(6117), 292–296.
759 https://doi.org/10.1126/science.1229953
760
761 Lundin R et al. (2004) Solar wind-induced atmospheric erosion at Mars: First results
762 from ASPERA-3 on Mars Express. Science, 305(5692) 1933–1936.
763
764 Lawrence DJ et al. (2019) Measuring the Elemental Composition of Phobos: The
765 Mars‐moon Exploration with GAmma rays and NEutrons (MEGANE) Investigation
766 for the Martian Moons eXploration (MMX) Mission Earth and Space Science, 6 2605–
767 2623. doi.org/10.1029/2019EA000811
768
769 Madey TE, Yakshinskiy BV, Ageev VN, Johnson RE (1998), Desorption of alkali
770 atoms and ions from oxide surfaces: Relative to the origins of Na and K in atmospheres
771 of Mercury and the Moon, J. Geophys. Res., 103(E3), 5873–5887.
772
773 Maruyama S, Ebisuzaki T (2017) Origin of the Earth: A proposal of new model called
774 ABEL, Geoscience Frontiers, 8(2), 253-274 doi.org/10.1016/j.gsf.2016.10.005
775
776 Matsumoto T, Harries D, Langenhorst F, Miyake A, Noguchi T (2020), Iron whiskers
777 on asteroid Itokawa indicate sulfide destruction by space weathering, Nature
778 Communications 11: 1117 doi.org/10.1038/s41467-020-14758-3
779
780 Matsuoka A, et al. (2018) The ARASE (ERG) magnetic field investigation, Earth,
781 Planets and Space, 70:43 doi.org/10.1186/s40623-018-0800-1
782
783 McComas DJ and Nordholt JE (1990) New approach to 3-D, high sensitivity, high mass

784 resolution space plasma composition measurements, Rev. Sci. Instrum. 61(10), 3095.
785 doi.org/10.1063/1.114169
786
787 McComas DJ, Allegrini F, Bochsler P, Frisch P, Funsten HO, Gruntman M, Janzen PH
788 et al. (2009) Lunar backscatter and neutralization of the solar wind: first observations of
789 neutral atoms from the Moon, Geophysical Research Letters, 36 (12), 2-5
790 doi.org/10.1029/2009GL038794
791
792 McElroy MB, Yung YL (1976) Oxygen isotopes in the Martian atmosphere:
793 Implications for the evolution of volatiles. Planet. Space Sci. 24, 1107–1113.
794 doi:10.1016/0032-0633(76)90148-3
795
796 McFadden JP et al. (2015) MAVEN SupraThermal and Thermal Ion Compostion
797 (STATIC) Instrument, Space Sci. Rev. 195, 199—256, doi.org/10.1007/s11214-015-
798 0175-6
799
800 Milillo A, et al. (2020), Investigating Mercury's Environment with the Two-Spacecraft
801 BepiColombo Mission, Space Sci. Rev., 216:93, doi.org/10.1007/s11214-020-00712-8
802
803 Miyoshi Y et al. (2018) Geospace exploration project ERG, Earth Planets Space, **70**:101
804 doi.org/10.1186/s40623-018-0862-0
805
806 Mordovskaya VG, Oraevsky VN, Styashkin VA (2001) Experimental evidence of the
807 Phobos magnetic field. Jetp Lett. 74, 293–297. https://doi.org/10.1134/1.1421402
808
809 Mura A, Milillo A, Orsini S, Kallio E, Barabash S (2002) Energetic neutral atoms at
810 Mars 2. Imaging of the solar wind - Phobos interaction, J. Geophys. Res., 107, 10:1278,
811 doi:10.1029/2001JA000328
812
813 Murata N, Karo H, Sasada I, and Shimizu T (2018) Fundamental Mode Orthogonal
814 Fluxgate Magnetometer Applicable for Measurements of DC and Low-Frequency
815 Magnetic Fields. IEEE Sensors Journal, 18, 2705-2712.
816

817 Murata N, Nomura R, and Matsuoka A (2019) Current annealing of amorphous wire
818 core for performance improvement of fundamental mode orthogonal fuxgate. Journal of
819 Magnetism and Magnetic Materials, 484, 497-503.
820
821 Nakamura T et al. Scientific observation plan of Phobos and Deimos from MMX
822 spacecraft, this issue.
823
824 Nénon Q et al. (2019) Phobos surface sputtering as inferred from MAVEN ion
825 observations. Journal of Geophys. Res.: Planets 124, 3385-3401.
826
827 Nishino MN et al. (2009), Solar-wind proton access deep into the near-Moon wake,
828 Geophys. Res. Lett., 36, doi.org/10.1029/2009GL039444
829
830 Nishino MN et al. (2010), Effect of the solar wind proton entry into the deepest lunar
831 wake, Geophys. Res. Lett., 37, doi.org/10.1029/2010GL043948
832
833 Nishino MN et al. (2013), Type-II entry of solar wind protons into the lunar wake:
834 Effects of magnetic connection to the night-side surface, Planetary Space Sci., 87,
835 106—114. doi.org/10.1016/j.pss.2013.08.017
836
837 Nishino MN et al. (2017) Kaguya observations of the lunar wake in the terrestrial
838 foreshock: Surface potential change by bow-shock reflected ions, Icarus, 293, 45—51.
839 doi.org/10.1016/j.icarus.2017.04.005
840
841 Nittler LR, McCoy TJ, Clark PE, Murphy ME, Trombka JI, Jarosewich E (2004) Bulk
842 element compositions of meteorites: A guide for interpreting remote‐sensing
843 geochemical measurements of planets and asteroids. Antarctic Meteorite Research, 17,
844 231– 251.
845
846 Ogohara K et al. The Mars system revealed by the Martian Moons eXploration mission,
847 this issue.
848
849 Øieroset M et al. (2010), Search for Phobos and Deimos gas/dust tori using in situ

observations from Mars Global Surveyor MAG/ER, Icarus, 206:189-198, doi.org/10.1016/j.icarus.2009.07.017

Ozima M, Seki K, Terada N, Miura YN, Podosek FA, Shinagawa H (2005) Terrestrial nitrogen and noble gases in lunar soils. Nature 436, 655–659.

Ozima M, Yin Q-Z, Podosekc FA, Miura, YN (2008) Toward understanding early Earth evolution: Prescription for approach from terrestrial noble gas and light element records in lunar soils. Proc. Natl Acad. Sci. 105, 17654–17658.

Pollock C et al. (2016) Fast Plasma Investigation for Magnetospheric Multiscale, Space Sci. Rev., 199(1), 331—406, doi.org/10.1007/s11214-016-0245-4

Pope SA, et al. (2011) Exploring planetary magnetic environments using magnetically unclean spacecraft: a systems approach to VEX MAG data analysis. Ann. Geophys., 29(4), 639-647.

Poppe AR, Curry SM, (2014) Martian planetary heavy ion sputtering of Phobos, Geophys. Res. Lett., 41(18), 6335-6341 doi.org/10.1002/2014GL061100

Poppe AR, Curry SM, Fatemi S (2016) The Phobos neutral and ionized torus, J. Geophys. Res. Planets, 121(5) 770—783 doi.org/10.1002/2015JE004948

Ramstad R, Barabash S, Futaana Y, Nilsson H, Holmström M. Global mars-solar wind coupling and ion es- cape. J. Geophys. Res., 122(8):8051–8062, 2017. doi: 10.1002/2017JA024306. URL http://dx.doi.org/10.1002/2017JA024306.

Richmond NC, Hood LL (2008), A preliminary global map of the vector lunar crustal magnetic field based on Lunar Prospector magnetometer data, J. Geophys. Res., 113, E02010, doi.org/10.1029/2007JE002933.

Rosenblatt P et al. (2016) Accretion of Phobos and Deimos in an extended debris disc stirred by transient moons. Nat. Geosci. 9, 581–583

Saito Y et al. (2020) Pre-flight Calibration and Near-Earth Commissioning Results of the Mercury Plasma Particle Experiment (MPPE) onboard MMO (Mio), Space Science Reviews, accepted.

Saito Y et al. (2012) Simultaneous Observation of the Electron Acceleration and Ion Deceleration over Lunar Magnetic Anomalies, Earth, Planets and Space, 64, 83–92, doi.org/10.5047/eps.2011.07.011

Saito Y et al. (2010) In-flight Performance and Initial Results of Plasma Energy Angle and Composition Experiment (PACE) on SELENE (Kaguya), Space Sci. Rev., 154(1-4), 265—303 doi.org/10.1007/s11214-010-9647-x

Saito Y et al. (2008a) Low energy charged particle measurement by MAP-PACE onboard SELENE, Earth, Planets and Space, 60, 375–385, doi.org/10.1186/BF03352802

Saito Y et al. (2008b) Solar wind proton reflection at the lunar surface: Low energy ion measurement by MAP-PACE onboard SELENE (KAGUYA), Geophys. Res. Lett., 35, L24205 doi.org/10.1029/2008GL036077

Saito Y, Yokota S, Asamura K (2017) High speed MCP anodes for high time-resolution low-energy charged particle spectrometers, J. Geophys. Res., 122(2), 1816—1830, doi.org/10.1002/2016JA023157

Sasada I (2002) Orthogonal fuxgate mechanism operated with dc biased excitation. Journal of Applied Physics, 91, 7789-7791.

Sasada I and Usui T (2003) Orthogonal Fluxgate Magnetometer Utilizing Bias Switching for Stable Operation. Proceedings of IEEE Sensors, 2, 468-471.

Sasaki S, Nakamura K, Hamabe Y, Kurahashi E, Hiroi T (2001) Production of iron

nanoparticles by laser irradiation in a simulation of lunar-like space weathering, Nature 410, 555–557 doi.org/10.1038/35069013

Schaible, MJ (2014). The role of solar wind in the formation of hydroxyl on airless silicate bodies in space (Master's thesis), Charlottesville, VA: University of Virginia.

Schaible MJ, Dukes CA, Hutcherson AC, Lee P, Collier MR, Johnson RE (2017) Solar wind sputtering rates of small bodies and ion mass spectrometry detection of secondary ions. J. Geophy. Res. Planets 122, 1968–1983. doi.org/10.1002/2017JE005359

Seki K, Elphic RC, Hirahara M, Terasawa T, Mukai T (2001) On atmospheric loss of oxygen ions from Earth through magnetospheric processes. Science 291, 1939–1941.

Sprenke KF, Baker LL (2000) Magnetization, Paleomagnetic Poles, and Polar Wander on Mars, Icarus 147, 26-34

Tanaka T et al. (2009) First in situ observation of the Moon-originating ions in the Earth's Magnetosphere by MAP-PACE on SELENE(KAGUYA), Geophys. Res. Lett., 36, L22106. doi.org/10.1029/2009GL040682

Taylor SR, Taylor GJ, Taylor LA (2006) The moon: A taylor perspective. Geochim. Cosmochim. Acta 70, 5904–5918.

Trotignon JG, Grard R, Barabash S, R.Lundin, E.Dubinin (1996),Solar wind measurements near Mars and their implication in the Red Planet environment, Planetary and Space Sci., 44(2), 117-127

Terada K, Yokota S, Saito Y, Kitamura N, Asamura K, Nishino MN (2017) Biogenic oxygen from Earth transported to the Moon by a wind of magnetospheric ions, Nature Astronomy, 1, 0026. doi:10.1038/s41550-016-0026

Terada K et al. (2018) Thermal and impact histories of 25143 Itokawa recorded in Hayabusa particles, Scientific Reports 8:11806 doi.org/10.1038/s41598-018-30192-4

Tsunakawa H, Shibuya H, Takahashi F, Shimizu H, Matsushima M, Matsuoka A, Nakazawa S, Otake H, Iijima Y (2010) Lunar magnetic field observation and initial global mapping of lunar magnetic anomalies by MAP-LMAG onboard SELENE(Kaguya). Rev. 154, 219–251.

Tsunakawa H, Takahashi F, Shimizu H, Shibuya H, Matsushima M (2015) Surface vector mapping of magnetic anomalies over the Moon using Kaguya and Lunar Prospector observations. J. Geophys. Res. 120, 1160–1185.

Usui T et al. (2020) The importance of Phobos sample return for understanding the Mars-moonsystem, Space Sci Rev 216:49, doi.org/10.1007/s11214-020-00668-9

Vernazza PR, Binzel P, Rossi A, Fulchignoni M, Birlan M (2009) Solar wind as the origin of rapid reddening of asteroid surfaces, Nature 458, 993.

Veselovsky IS (2004), Is Phobos Magnetized? Solar System Research 38, 188–193

Watanabe S et al. (2019), Hayabusa2 arrives at the carbonaceous asteroid 162173 Ryugu—a spinning top–shaped rubble pile. Science 364, 268–272

Wieser M et al. (2009), Extremely high reflection of solar wind protons as neutral hydrogen atoms from regolith in space. Planet. Space Sci. 57, 2132–2134.

Wilson A (eds) (2004) Mars Express: The Scientific Payload, (ESA Special Publication SP-1240

Yokota S, Saito Y (2005) Estimation of picked-up lunar ions for future compositional remote SIMS analyses of the lunar surface, Earth, Planets and Space, 57, 281—289 doi.org/10.1186/BF03352564

Yokota S, Saito Y, Asamura K, Mukai T (2005) Development of an ion energy mass spectrometer for application on board three-axis stabilized spacecraft. Rev Sci Instrum

982 76:014501–014508.
983
984 Yokota S et al. (2009) First direct detection of ions originating from the Moon by MAP-
985 PACE IMA onboard SELENE (KAGUYA). Geophys. Res. Lett. 36, L11201.
986
987 Yokota S et al. (2014) Structure of the ionized lunar sodium and potassium exosphere:
988 Dawn-dusk asymmetry, J. Geophys. Res., 119(4), 798—809
989 doi.org/10.1002/2013JE004529
990
991 Yokota S, Kasahara S, Mitani T, Asamura K, Hirahara M, Takashima T, Yamamoto K,
992 Shibano Y (2017) Medium-energy particle experiments – ion mass analyzer (MEP-i)
993 onboard ERG (Arase), Earth Planets Space, 69:172. doi.org/10.1186/s40623-017-0754-
994 8
995
996 Yokota S et al. (2020) Global emissions of indigenous carbon ions from the Moon,
997 Science Advances, 6, eaba1050 doi.org/10.1126/sciadv.aba1050
998

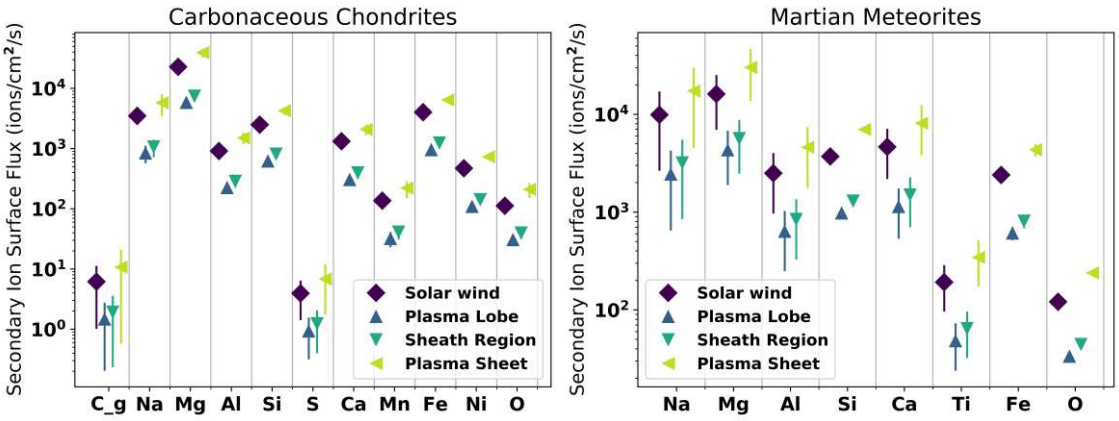

Figure 1: Secondary ion ratios for several types of meteorites considering the solar wind and Martian magnetospheric ion sputtering. Solar wind fluxes were calculated assuming 95% H+ and 5% He++ ions, and incident ion fluxes for the various magnetosphere regions were calculated using MAVEN SWIA measurements (J. Halekas, personal communication).

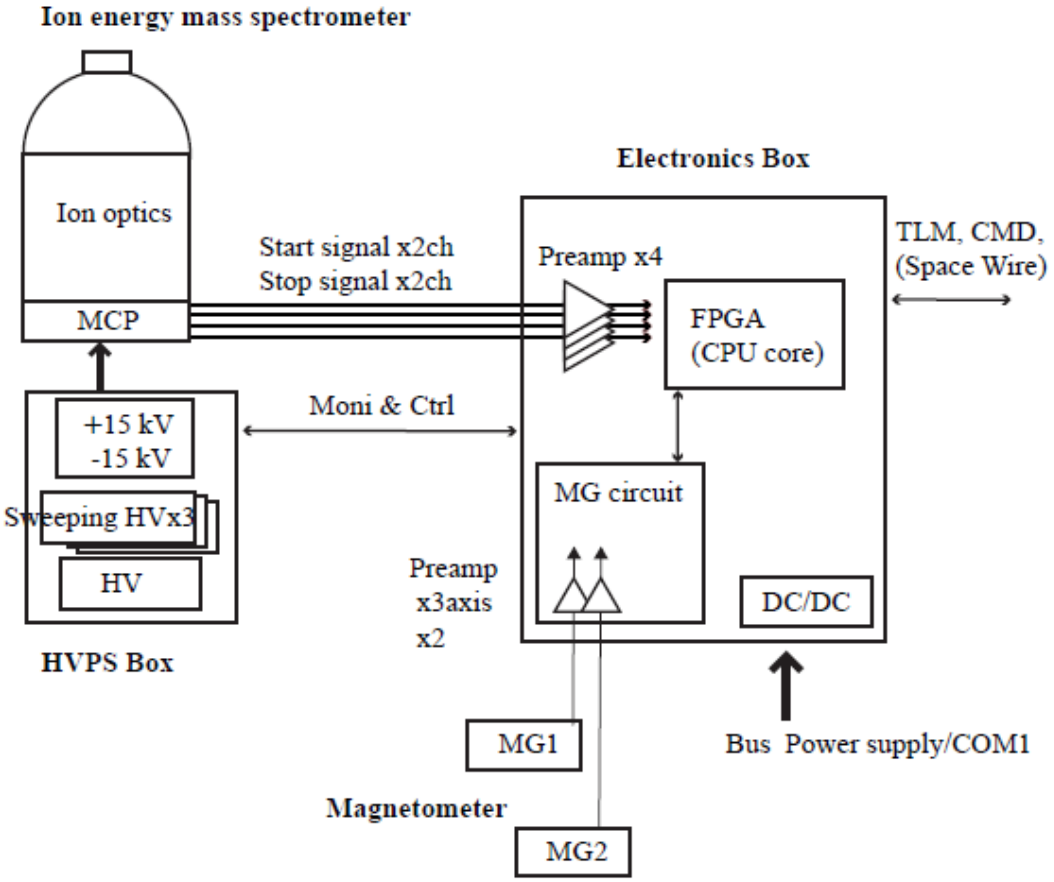

1008

1009 **Figure 2:** Block diagram of MSA.

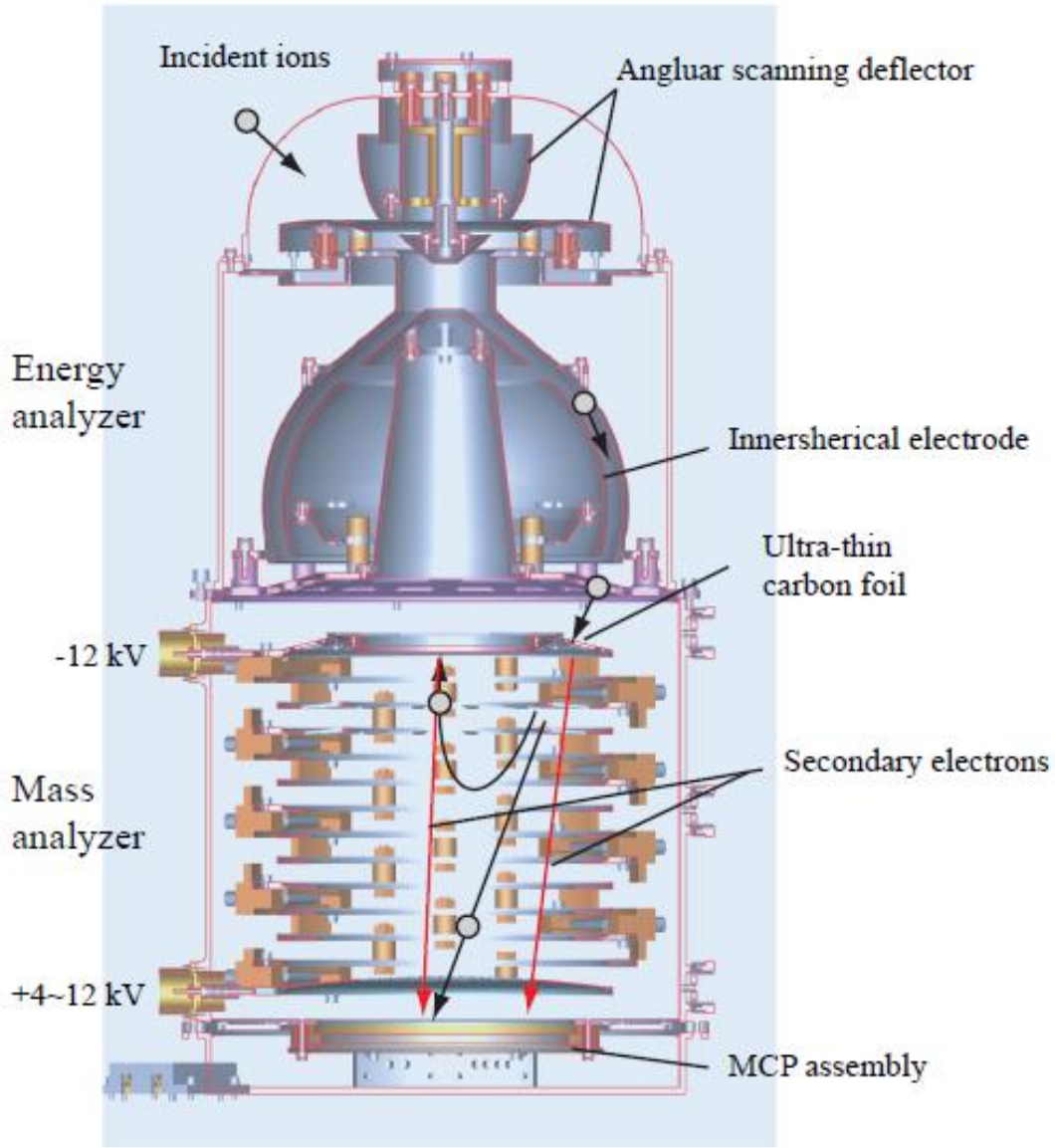

1010

1011 **Figure 3:** Cross-sectional view, of the ion optics and MCP assembly in the MSA ion
1012 energy mass spectrometer engineering model. Trajectories of incident ions (black) and
1013 secondary electrons (red) are shown.

1014

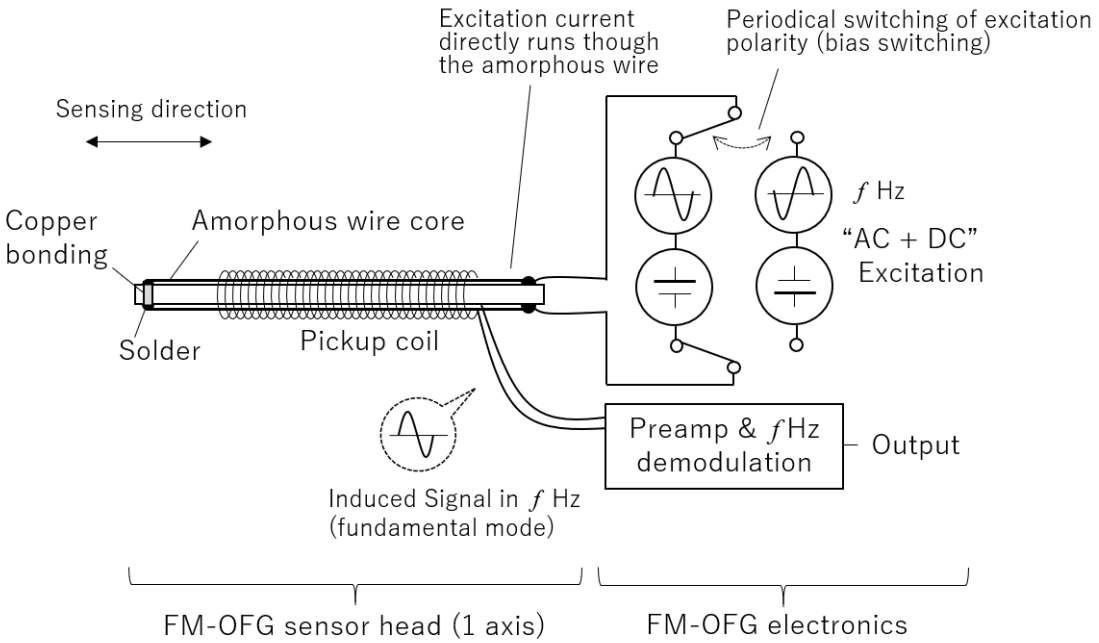

Figure 4: Schematic diagram of the MSA magnetometer.

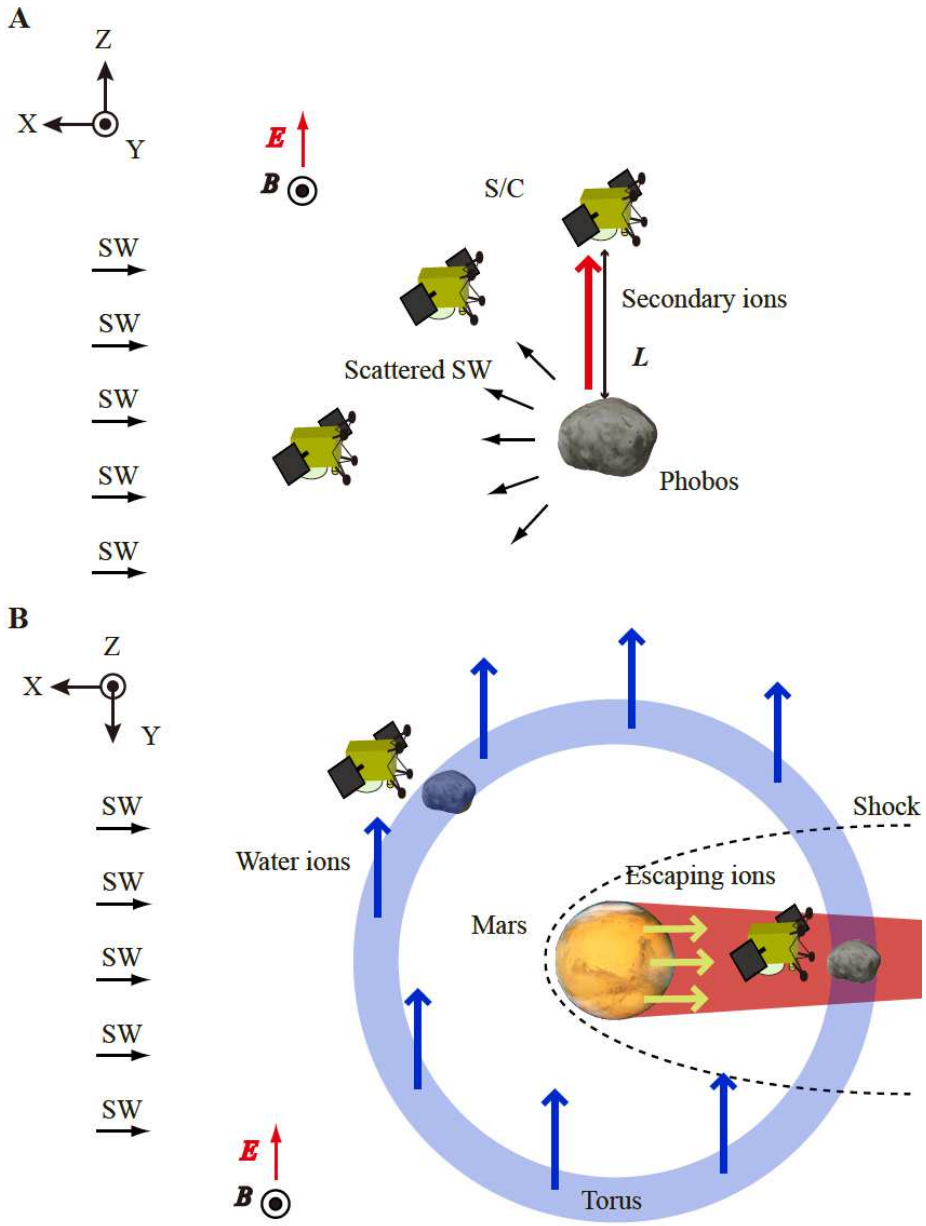

Figure 5: Observation configurations of MSA. A) MSA observations 1 and 3 for measuring solar wind (SW) ions, scattered SW ions on the Phobos surface, and secondary ions sputtered by the SW from Phobos surface. B) MSA observations 2 and 4 for measuring water ions from the torus and escaping ions from the Martian atmosphere. In the both panels, $\boldsymbol{B}$ and $\boldsymbol{E}$ indicate the magnetic and electric fields of the SW, respectively. The magnetometer measures $\boldsymbol{B}$, while $\boldsymbol{E}$ is derived from $\boldsymbol{E} = -\boldsymbol{V} \times \boldsymbol{B}$, where $\boldsymbol{V}$ denote the SW velocity measured by the ion analyzer. The Phobos/Mars-centric Solar Ecliptic coordinate system is used in panel A/B.

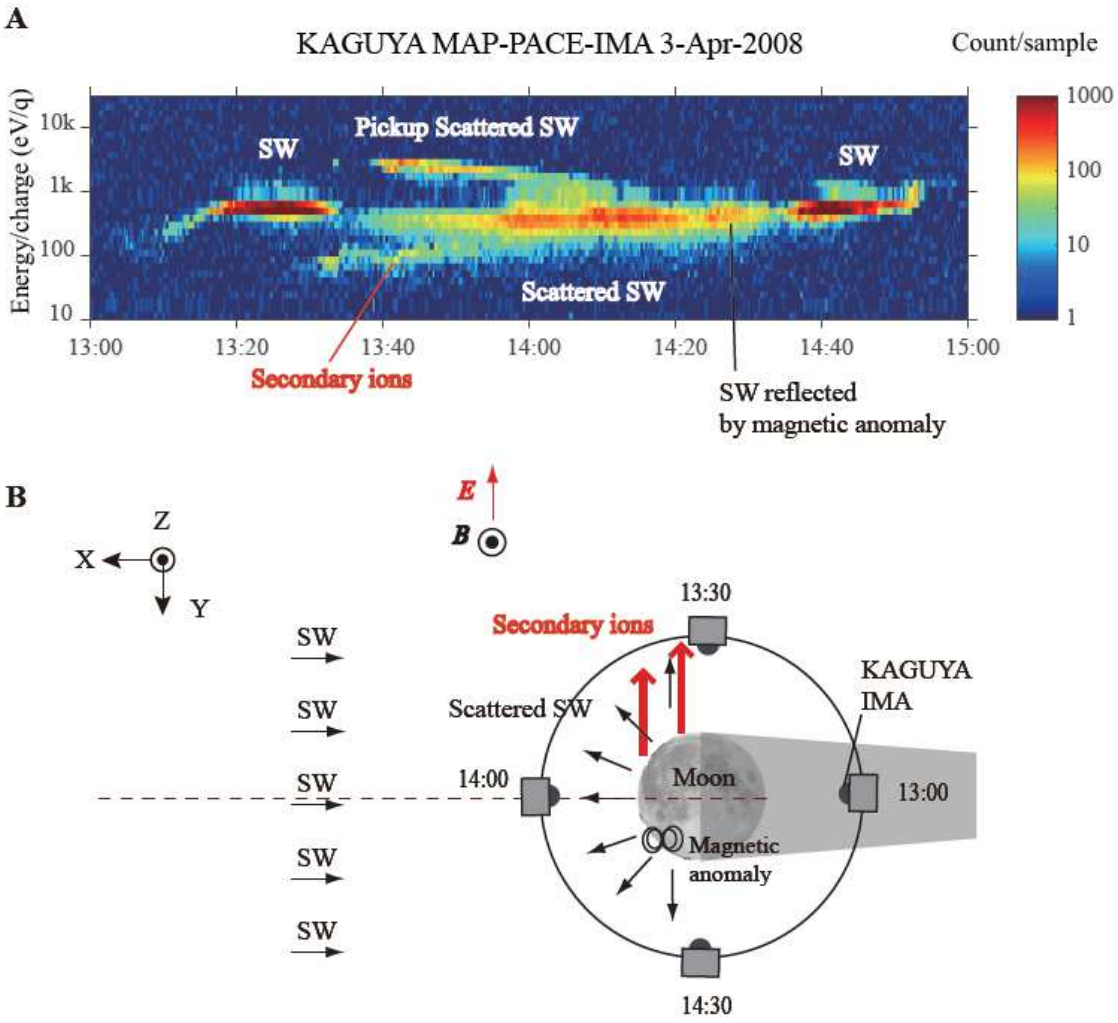

1027

1028 **Figure 6:** Ion observation results around the Moon by the Kaguya spacecraft during two
1029 hours on April 3, 2008. A) Energy-time spectrograms of ions measured by the ion
1030 analyzer (IMA) between 13:00 and 15:00 universal time (UT). B) Ion observation
1031 configuration in the selenocentric solar ecliptic coordinates. The details of the
1032 observations are described in Saito et al. (2010).

1033

1034

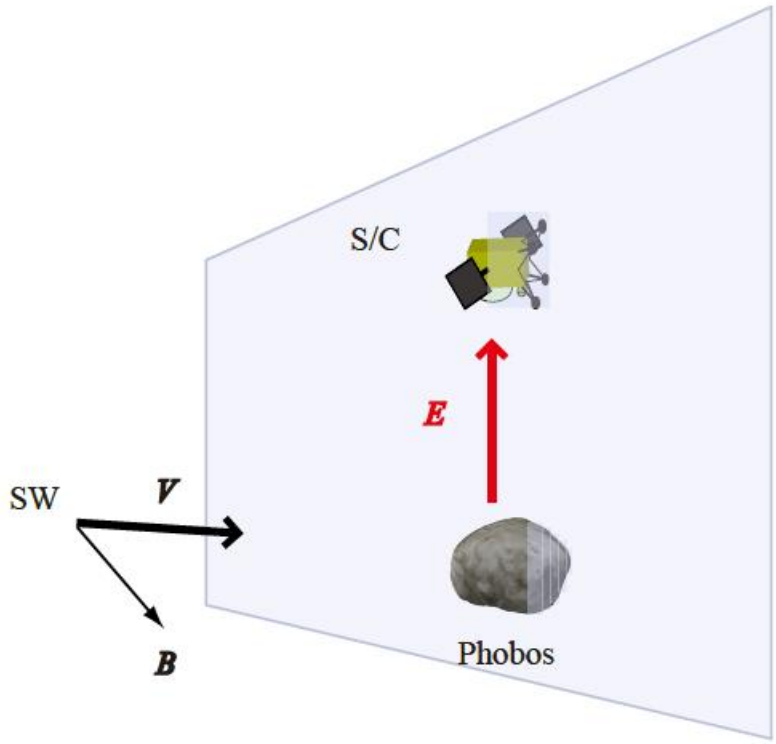

Figure 7: Required observation configuration for the MSA observation 1 to measure secondary ions sputtered by the solar wind (SW) from Phobos surface, where $\boldsymbol{V}$, $\boldsymbol{B}$, and $\boldsymbol{E}$ indicate the velocity, and magnetic and electric fields of the SW, respectively. The secondary ions move along $\boldsymbol{E} = -\boldsymbol{V} \times \boldsymbol{B}$, because their initial energies are nearly 0. The magnetometer measures $\boldsymbol{B}$, while $\boldsymbol{E}$ is derived from $\boldsymbol{E} = -\boldsymbol{V} \times \boldsymbol{B}$, where $\boldsymbol{V}$ denote the SW velocity measured by the ion analyzer. The spacecraft and Phobos are located in the same plane whose normal vector is $\boldsymbol{V}$.

Figures

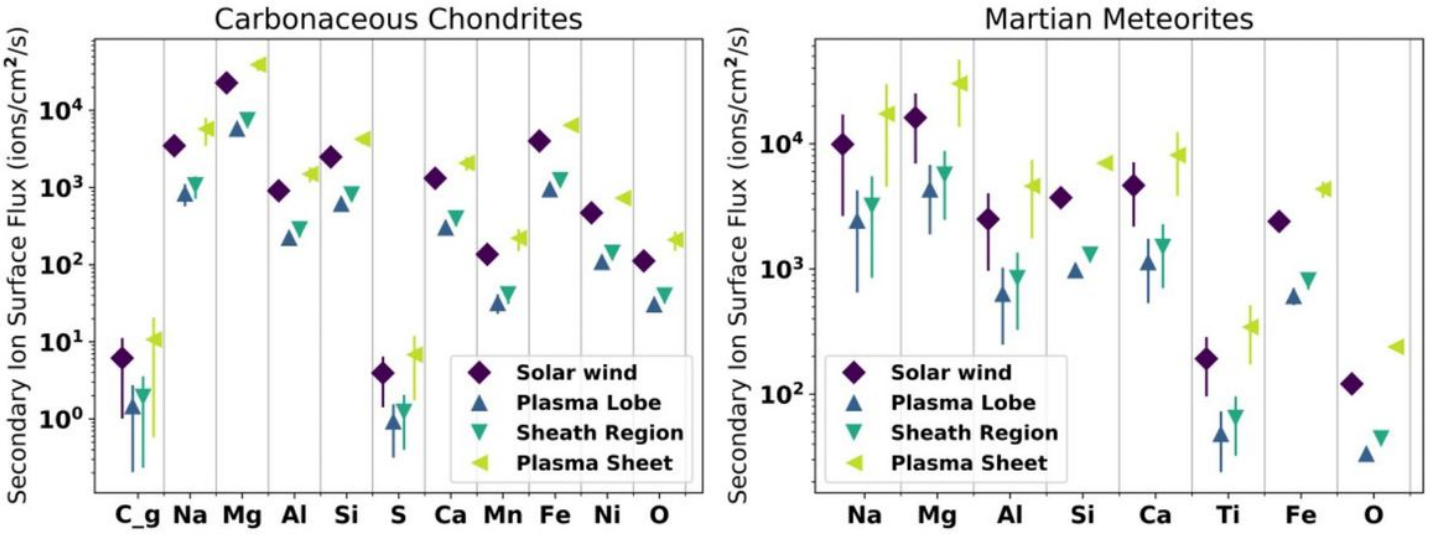

Figure 1

Secondary ion ratios for several types of meteorites considering the solar wind and Martian magnetospheric ion sputtering. Solar wind fluxes were calculated assuming 95% H+ and 5% He++ ions, and incident ion fluxes for the various magnetosphere regions were calculated using MAVEN SWIA measurements (J. Halekas, personal communication).

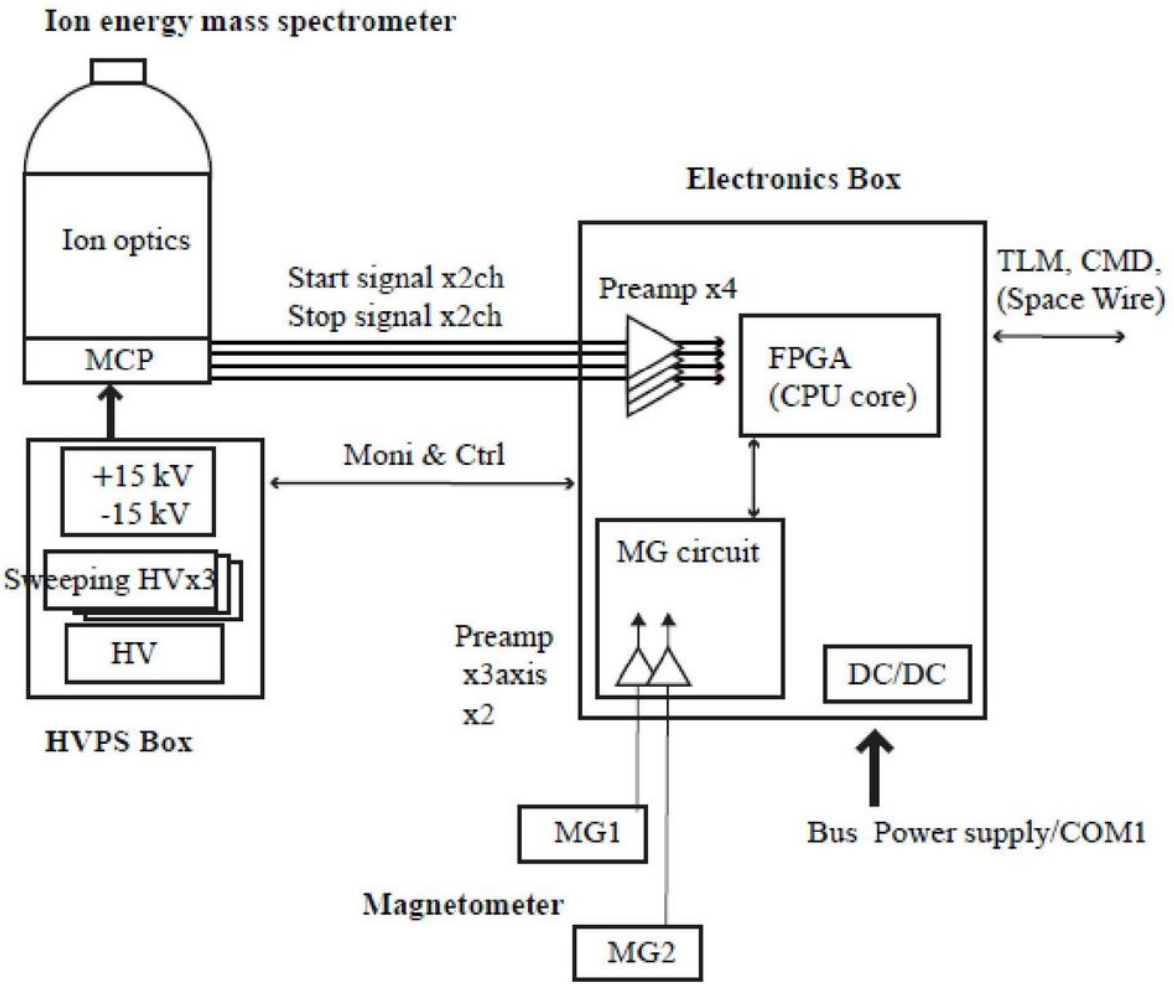

Figure 2

Block diagram of MSA.

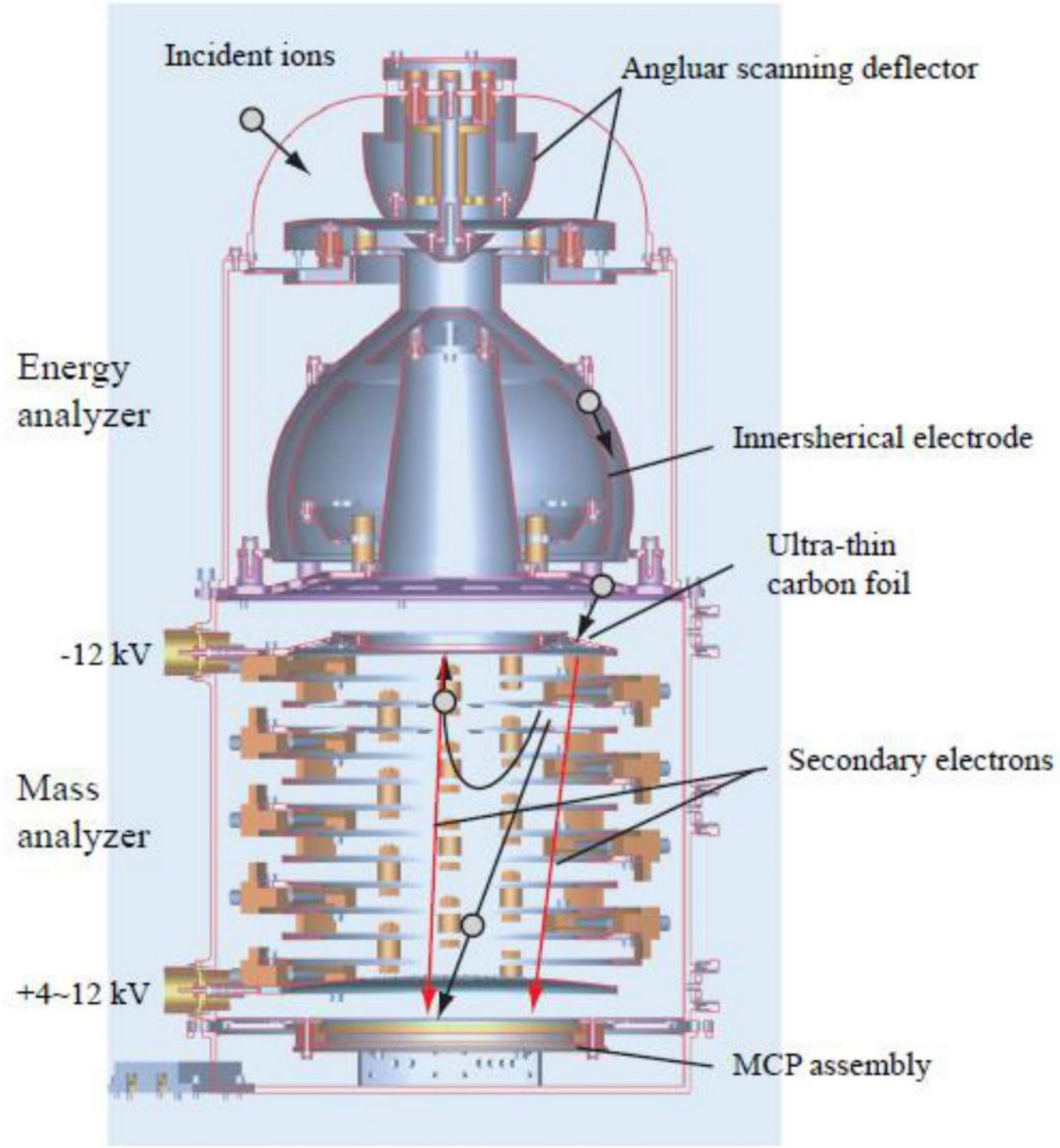

Figure 3

Cross-sectional view, of the ion optics and MCP assembly in the MSA ion energy mass spectrometer engineering model. Trajectories of incident ions (black) and secondary electrons (red) are shown.

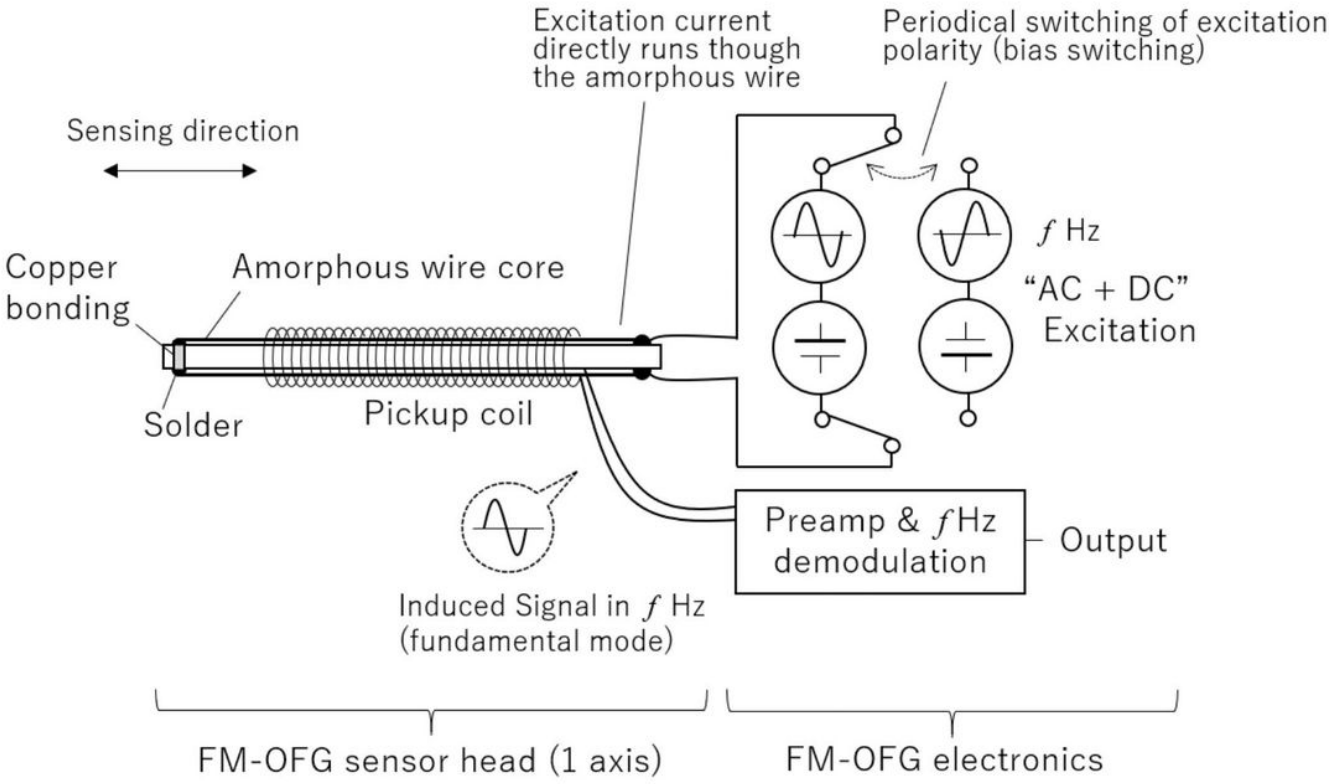

Figure 4

Schematic diagram of the MSA magnetometer.

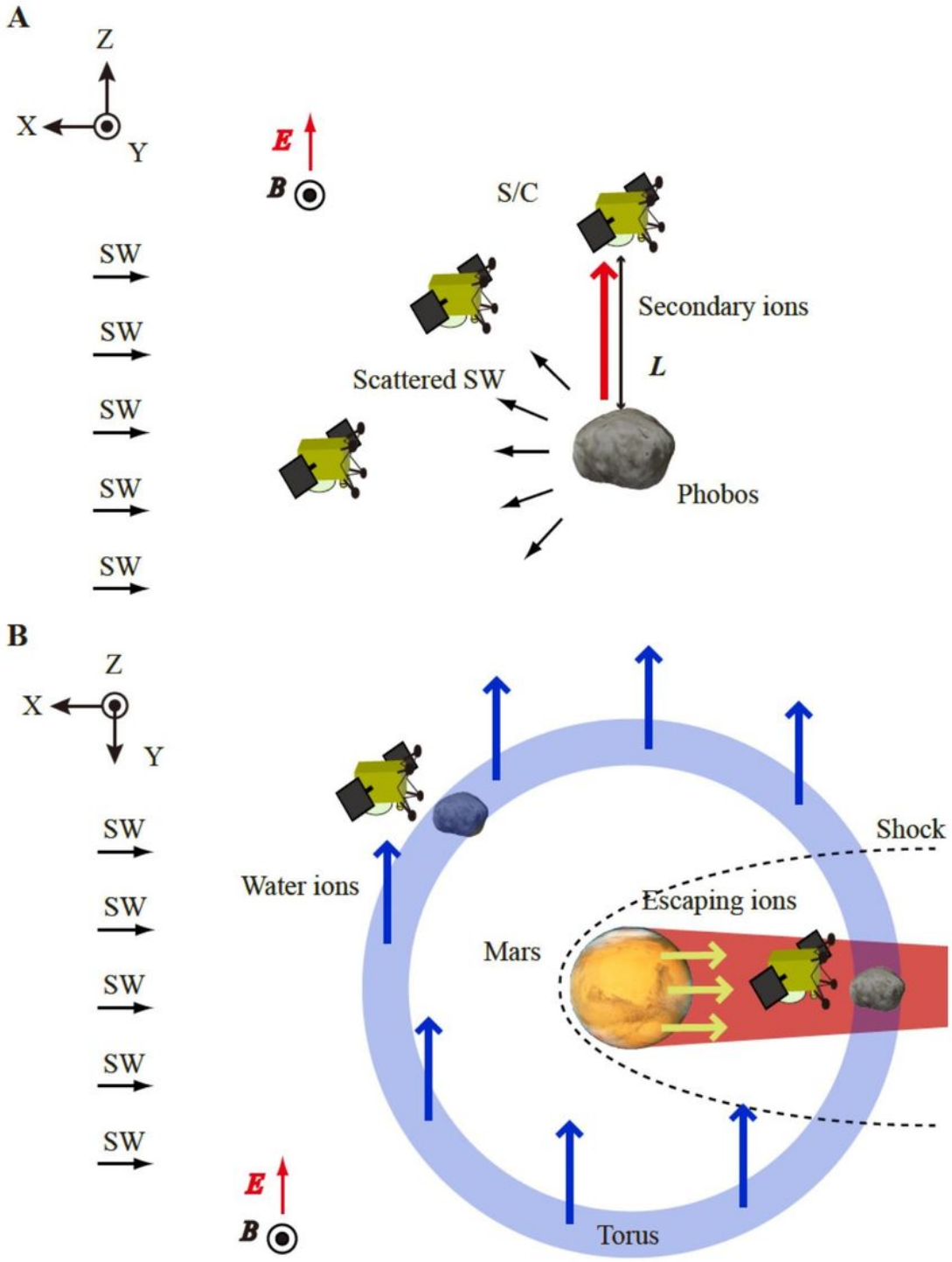

Figure 5

Observation configurations of MSA. A) MSA observations 1 and 3 for 1018 measuring solar wind (SW) ions, scattered SW ions on the Phobos surface, and secondary ions sputtered by the SW from Phobos surface. B) MSA observations 2 and 4 for measuring water ions from the torus and escaping ions from the Martian atmosphere. In the both panels, 𝑩 and 𝑬 indicate the magnetic and electric fields of the SW, respectively. The magnetometer measures 𝑩, while 𝑬 is derived from 𝑬 = −𝒗 × 𝑩, where 𝒗 denote the SW

velocity measured by the ion analyzer. The 1024 Phobos/Mars-centric Solar Ecliptic coordinate system is used in panel A/B.

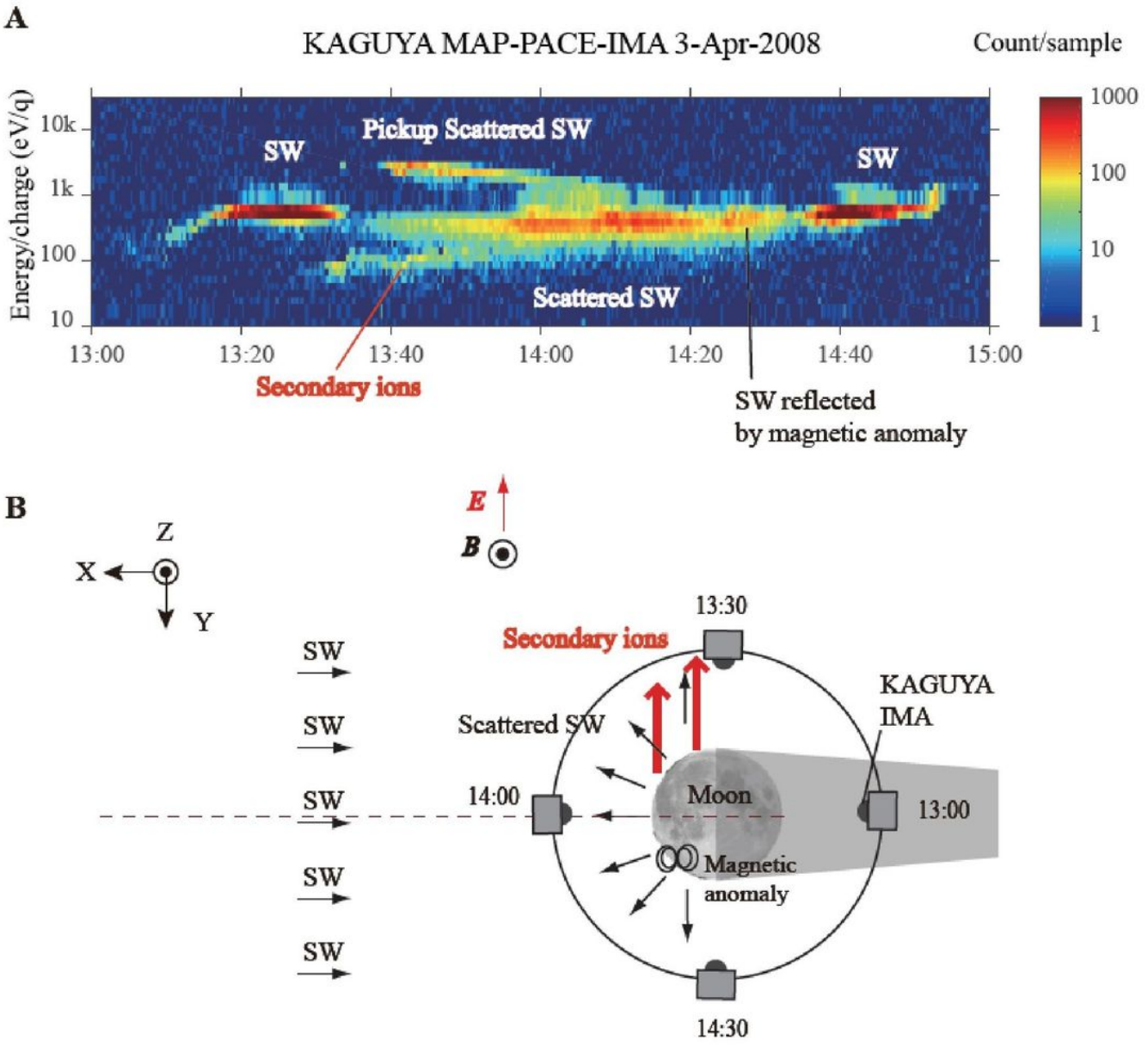

Figure 6

Ion observation results around the Moon by the Kaguya spacecraft during two hours on April 3, 2008. A) Energy-time spectrograms of ions measured by the ion analyzer (IMA) between 13:00 and 15:00 universal time (UT). B) Ion observation configuration in the selenocentric solar ecliptic coordinates. The details of the observations are described in Saito et al. (2010).

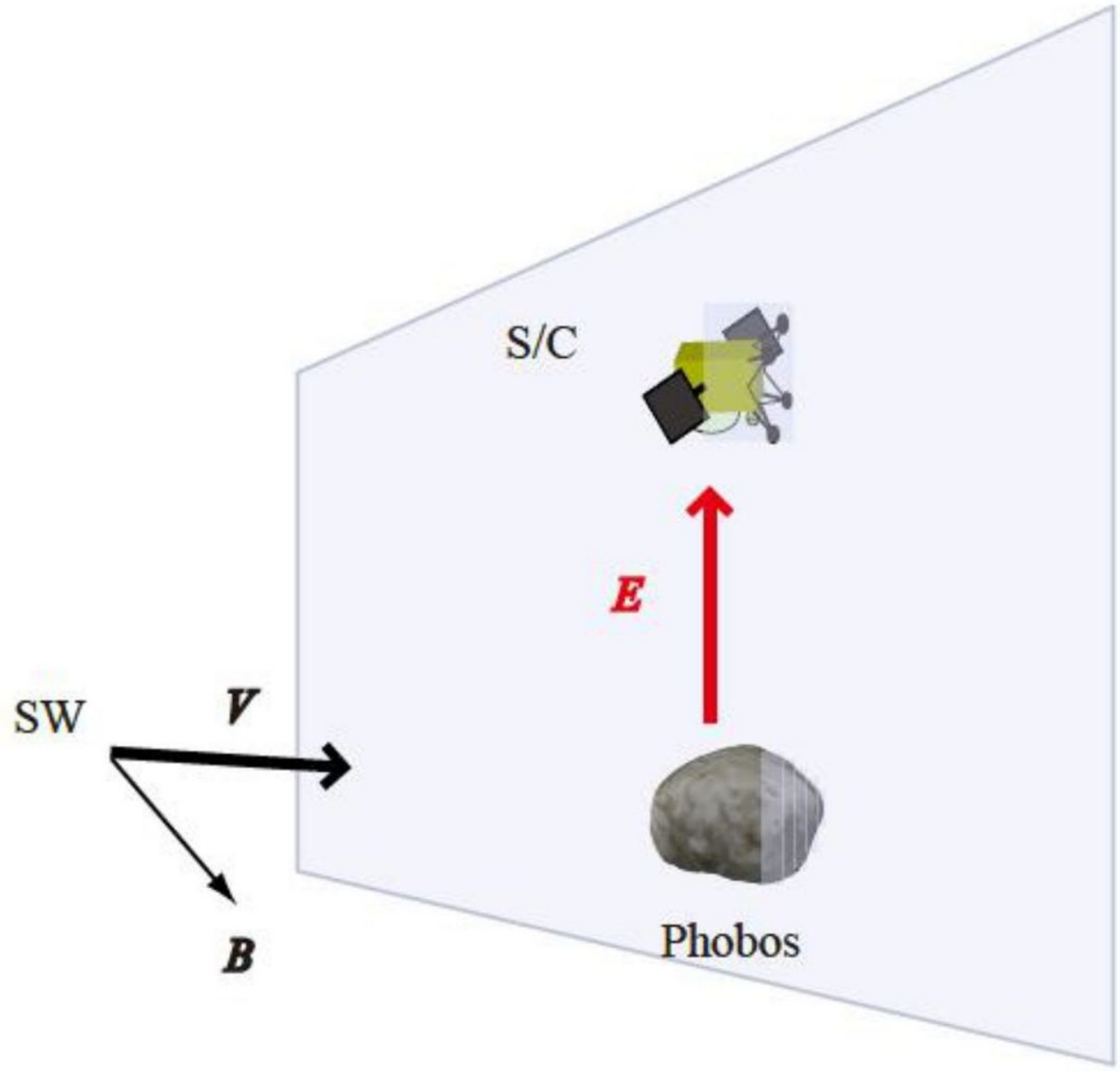

Figure 7

Required observation configuration for the MSA observation 1 to measure secondary ions sputtered by the solar wind (SW) from Phobos surface, where 𝑽, 𝑩, and 𝑬 indicate the velocity, and magnetic and electric fields of the SW, respectively. The secondary ions move along 𝑬 = −𝑽 × 𝑩, because their initial energies are nearly 0. The magnetometer measures 𝑩, while 𝑬 is derived from 𝑬 = −𝑽 × 𝑩, where 𝑽 denote the SW velocity measured by the ion analyzer. The spacecraft and Phobos are located in the same plane whose normal vector is 𝑩.

Supplementary Files

This is a list of supplementary files associated with this preprint. Click to download.

- gabst.png